Characterizing Inhibition of the CyclinA2-CDK2 Complex by Small Molecular Inhibitors using Two-dimensional NMR Spectroscopy

Undergraduate Honors Research Thesis

Presented in Partial Fulfillment of the Requirements for Graduation with Research Distinction in Biochemistry in the School of Arts and Sciences at The Ohio State University

Lauren Rager

Undergraduate Biochemistry Major

College of Arts and Sciences

The Ohio State University

2021

Project Advisor:

Dr. Mark P Foster, Department of Chemistry and Biochemistry

Table of Contents:

Abstract:

CyclinA2 is best known for the regulation of the eukaryotic cell cycle through binding and activating CDK2. The role of the CyclinA2-CDK2 protein complex as a regulator of the S and G2 phases of the cell cycle is well characterized, but additional functions of these proteins when acting independently is more enigmatic. While both proteins operate separately in DNA damage repair pathways, CyclinA2 has additionally been implicated in neuronal development and maintenance, working apart from CDK2. Development and application of CyclinA2-specific inhibitors will elucidate the protein's specific roles in the neuron. Prior computational modeling done by Dr. Stephanie Kim identified four potential small molecule inhibitors which were intended to act on an allosteric site of CyclinA2, and were confirmed to be inhibitory with an assay testing the activity of the CyclinA2-CDK2 complex. Our aim was to determine where these inhibitors interact with the CyclinA2-CDK2 complex using 2D ^{1}H-^{15}N NMR spectroscopy. Comparison of the NMR spectra of CDK2 in the presence of ATP and three of the inhibitors indicated that CDK2 interacts with these inhibitors independently of CyclinA2. Furthermore, similarities in the titration spectra of the compounds and ATP suggest that these molecules may act competitively at the ATP binding site. Efforts to determine how CyclinA2 or the CyclinA2-CDK2 complex interacted with the compounds were inconclusive.

Acknowledgements:

I express my deepest thanks to my research advisor, Dr. Mark P Foster, who provided invaluable insight and support over the past two years. Despite entering the lab with no background in NMR, his encouragement has motivated me to meet the challenge of confronting a new field, and inspired me to integrate research into my professional career post-graduation. I would also like to thank Dr. Deepak Kumar Yadav, for his exceptional mentorship throughout this investigation. His instruction in wet lab skills, data interpretation, and the application of the scientific method has been instrumental in my growth as a researcher and a critical thinker.

Furthermore, I would like to thank Kye Stachowski for his continued support and encouragement, as well as the other members of the Foster Lab. My experience conducting research with them has taught me much about effective scientific communication and collaboration on both a small and large scale, and I have thoroughly enjoyed my time in the lab.

Finally, I would like to thank Dr. Jose Otero and Dr. Stephen Lindert for their interdisciplinary collaboration with me on this project, and Dr. Jane Jackman and Dr. Michael Weinstein for serving on my defense committee.

1. Introduction

The eukaryotic cell cycle is imperative in embryological development, tissue regeneration, and growth. Cyclin-dependent kinases (CDK) and their regulatory counterparts, Cyclins, are responsible for checkpoint mediation throughout the cell cycle in the G1, S, G2, and M phase (Figure 1A). Upon complex formation with a cognate CDK, each member of the cyclin family regulates specific aspects of transcription and cellular replication (Figure 1B). Cyclins are then tagged for ubiquitin-mediated proteolysis, resulting in a decrease in the corresponding kinase activity (Brown et al., 1999).

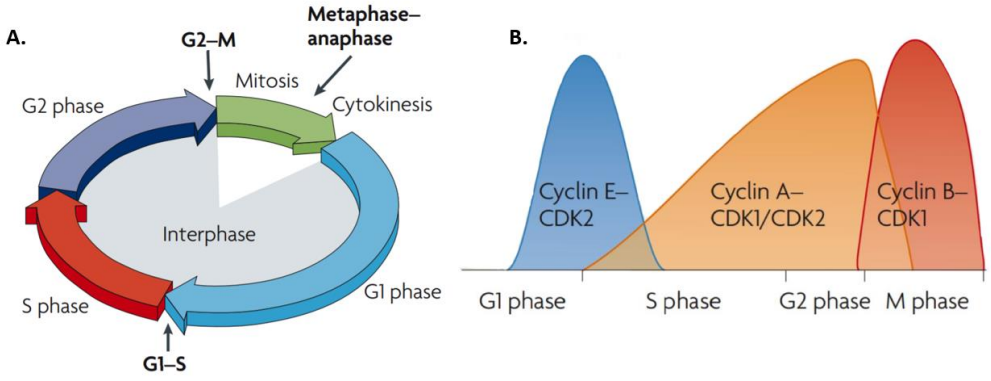

Figure 1: Cyclin-CDK complexes regulate the cell cycle. **A**. The cell cycle includes both interphase and mitosis. Interphase can be further divided into G1 phase, S phase, and G2 phase. The checkpoints marked G1-S and G2-M are regulated by Cyclin-CDK complexes. **B.** The distribution of Cyclin-CDK complexes throughout the cell cycle is visualized. Different combinations of Cyclins and CDKs phosphorylate key proteins at each checkpoint. Figure adapted from Hochegger et al., 2008.

The CyclinA2-CDK2 complex is responsible for initiation of DNA replication in the S phase, specifically via the phosphorylation of key proteins (Kanakkanthara et al., 2016; Li et al., 2015). Both CDK2 and CyclinA2 are known to interact with other associated proteins, leading to various cellular functions. CDK2 is involved in chromatin remodeling and apoptosis, and is essential in instigating the DNA Repair Response (DRR) network to repair DNA damage due to radiation, oxidative damage, and chemical mutagens (Liu et al., 2020). The C-terminus of CyclinA2, which shows low sequence homology with other members of the Cyclin family, binds to the UTR of Mre11 transcripts, promoting translation of Mre11, a protein instrumental in repair of DNA double stranded breaks. Mice unable to regulate normal concentrations of cellular CyclinA2 were shown to be more likely to develop tumors due to a lack of this ability (Kanakkanthara et al., 2016).

Additionally, CyclinA2 has been shown to be important in neuronal development and functioning. In neural cells obtained from mice, a deficit of CyclinA2 resulted in neurological developmental impediments (Otero et al., 2014). In addition, the decreased regulation of chromosomal duplication and hindered DNA repair mechanisms in embryogenesis caused increased apoptosis and lengthened the cell cycle, resulting in delayed proliferation of the forebrain (Gygli et al., 2016). Furthermore, different isoforms of CyclinA2 have been identified in the brain during different points in development. In embryonic mice, the predominant form was full length CyclinA2 protein, indicating importance in neural proliferation; while a truncated isoform without the N-terminus was determined to be present in adult mice, suggesting a role in neuronal maturation (Otero et al., 2014). Adult mice shown to be deficient in CyclinA2 displayed learning and memory deficits, consistent with an inability to repair double stranded DNA breaks in mature neurons in the hippocampus (Gygli et al., 2016). CDK2 is not required for hippocampal

neurogenesis and maintenance, and CDK2-deficient mice displayed no significant difference in proliferation of neuron-progenitor cells or differentiation (Vandenbosch et al., 2008).

Structurally, CyclinA2 is composed of twelve α-helices. Much like other members of the Cyclin family, CyclinA2 contains a Cyclin fold, two structurally identical sets of five α-helices separated by a linker of five amino acids. These α-helices pack loosely in a globular structure (Figure 2A). Another structural feature of CyclinA2 is the Cyclin box, which mediates complex formation with CDK2 (Jeffrey et al., 1995). CDK2 is a globular protein, composed of two lobes with an ATP and Cyclin binding cleft in between (Figure 2A, 2B). Other components involved in complex formation involve the PSTAIRE helix, which interacts with the Cyclin box and is thought to be responsible for specificity; and the T-loop, which blocks the binding cleft in the absence of Cyclin (Jeffrey et al., 1995). Conformational changes in the presence of ATP and CyclinA2 include rotation of the PSTAIRE helix, resulting in a tighter protein structure of CDK2, and the movement of the T-loop away from the bi-lobar protein body (Figure 2A). This movement exposes the ATP binding cleft and conserved phosphorylation site at Thr160, and triggers CDK2 activation. Compared to the conformational changes undergone by CDK2, the structure of CyclinA2 remains relatively the same, with the Cyclin box and N terminal helices forming most of the interactions with CDK2 (Jeffrey et al., 1995).

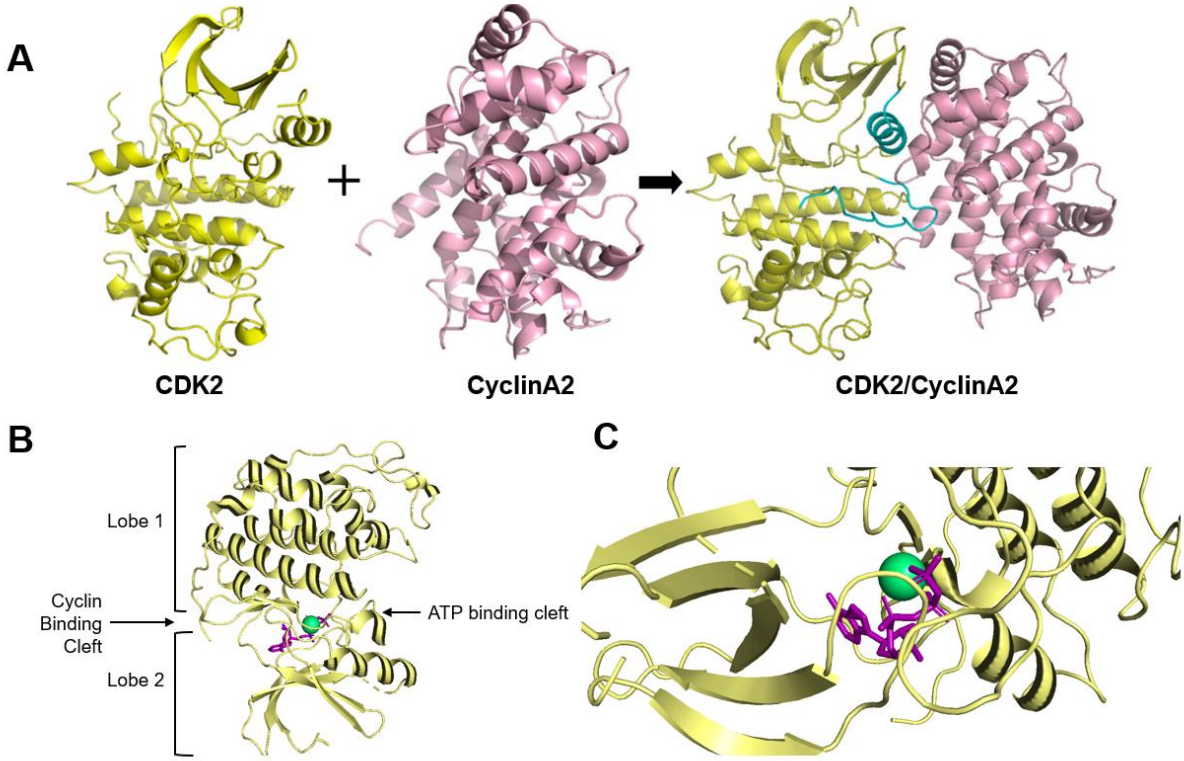

Figure 2: The Structure of CDK2 and the CyclinA2-CDK2 complex. **A.** Formation of the CyclinA2-CDK2 complex. CyclinA2 (PDB id 1FIN) and CDK2 (PDB id 1HCK) are pictured independently. Structural motifs of CDK2 which have undergone significant conformational changes upon binding to CyclinA2 is highlighted in cyan (PDB id 1OL1). These elements include shifting of the PSTAIRE helix and T-loop to facilitate phosphorylation activity. Figure from Li et al., 2015. **B**. Ribbon structure of CDK2 complexed with ATP and a magnesium ion. The bi-lobal structure, Cyclin box, and ATP binding cleft are indicated. **C.** A closer image of ATP-bound CDK2. ATP and the complexed magnesium ion can be seen buried in the binding cleft. Both B and C were created in pymol, with PDB id 1B39.

As both CyclinA2 and CDK2 have various roles in cell cycle regulation, DNA repair, and embryogenesis, development of Cyclin and CDK inhibitors is of great pharmacological interest. The vast majority of CDK inhibitors compete with ATP at the ATP binding site. Due to the highly conserved nature of the ATP binding pocket, current inhibitors are poor candidates as they lack specificity within the CDK family. Therefore, development of inhibitors that target allosteric sites on CDKs or the Cyclin binding partner would enable a greater degree of specificity. To our best knowledge, there are no inhibitors that specifically target CyclinA2, and there is only one inhibitor that targets an allosteric site on CDK2 (Faber et al., 2020).

The role of CyclinA2 in brain development has not yet been completely understood, and elucidating its functions without CDK binding partners is critical. Development of a CyclinA2 specific inhibitor would enable further investigation of the roles of CyclinA2 in the brain as well other capacities where it functions independently, and would be of great pharmacological interest. Computational structural modeling determined a potential allosteric binding site on CyclinA2, and identified several compounds which had inhibitory potential. Bioluminescence enzymatic assays were implemented measuring the activity of the CyclinA2-CDK2 complex, and four compounds were determined to be inhibitory in micromolar to nanomolar concentrations (Figure 3) (Stephanie Kim et al., 2020). However, as inhibitory capability was determined by measuring the kinase activity of the CyclinA2-CDK2 complex, it was unclear whether the inhibitors were binding to CyclinA2, or CDK2. Using Nuclear Magnetic Resonance (NMR) spectroscopy and native Mass Spectrometry, we aim to identify where these molecular inhibitors interact with the complex. By recording ^{15}N-HSQC NMR data and measuring chemical shift perturbations of the amide backbone signals, which indicate ligand-protein interactions, we confirm that all three inhibitors

which were tested interact with CDK2, and potentially inhibit activity through binding at the ATP binding site.

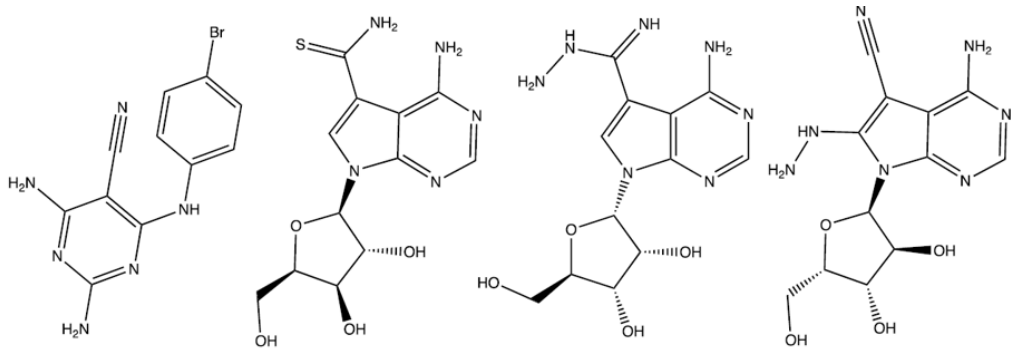

	1	2	3	4
	NSC71866	NSC105827	NSC107517	NSC172599
IC50 values:	6.5 µM	7.6 nM	181 nM	1.9 µM

Figure 3: Designed molecular inhibitors of CDK2. The four inhibitors determined to bind to the allosteric sit on CyclinA2 are pictured above. The NSC identification numbers are listed below each compound, as are the IC50 values, determined by the *in vitro* biochemical assay.

2. Methods and Materials

2.1. Subcloning of CyclinA2 and CDK2 to engineer MBP fusion proteins

Preliminary expression and purification attempts for CyclinA2 resulted in precipitation of the protein. It has been reported that CyclinA2 can be successfully expressed in *E. coli* with the use of molecular folding chaperones (Grigoroudis et al., 2015). Furthermore, solubility of

expressed proteins with poor yield can be increased with the fusion of Maltose Binding Protein to the passenger protein within a pHMT vector (Figure 4a). Fusion of protein with MBP, along with a 6xHis metal affinity tag and TEV cleavage site allows for increased solubility and easy purification of the protein from the MBP-6xHis construct (Kapust & Waugh, 1999).

DNA plasmids containing genes encoding the human CyclinA2 and Cyclin Dependent Kinase 2 proteins were received from Dr. Richard W. Kriwacki's lab at St. Judes Children's Hospital. The pHMT vector consisted of a 6xHis tag to aid in purification, a TEV cleavage site to sever the metal affinity tag and MBP from the protein of interest, and an MBP fusion protein, as well as a gene for Ampicillin resistance (Figure 4B). The protein insert would be ligated at the *EcoRI* and *HindIII* restriction digestion sites (Figure 4C).

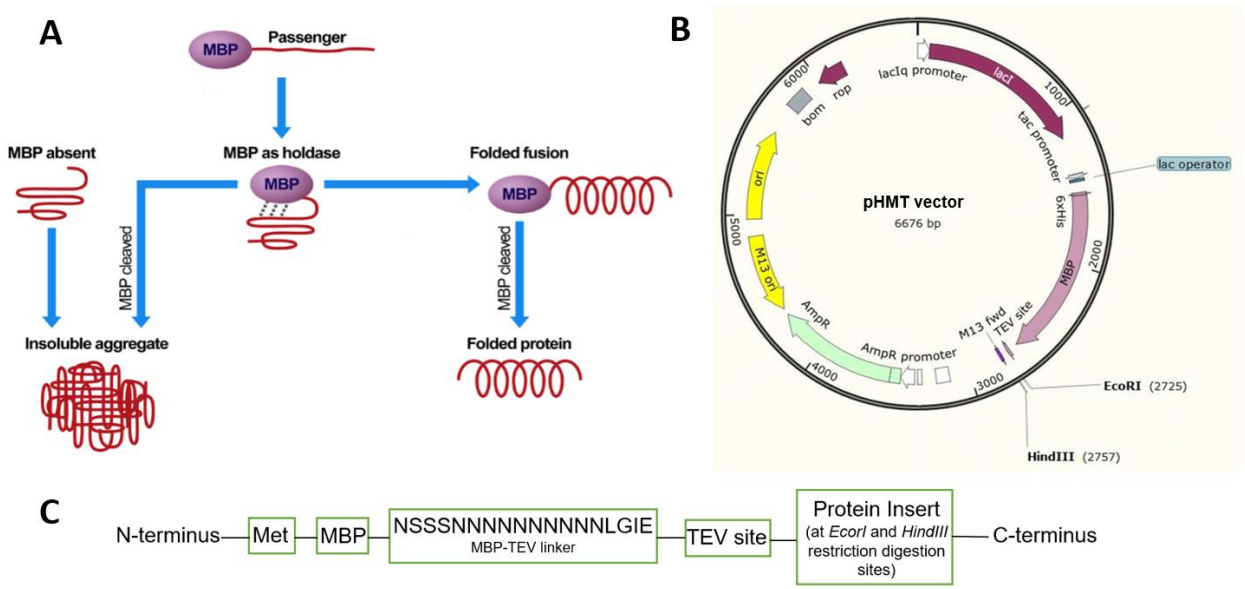

Figure 4: MBP fusion can increase solubility of proteins. **A.** Fusion of a passenger protein to MBP prevents insoluble aggregation of the protein of interest. Adapted from Kapust and Waugh, 1999. **B.** A pHMT vector can be used for expression of the protein of interest. MBP is fused to a

6xHis tag, and separated from the ligation point (marked by restriction enzyme sites of *EcoRI* and *HindIII*) by a TEV site. **C.** The expressed fusion protein includes the MBP protein, the TEV cleavage site, and the protein insert.

2.1.1. Amplification of CyclinA2 and CDK2 by polymerase chain reaction

PCR was performed with the CyclinA2 and CDK2 templates, and primers were designed to include the *EcoRI* restriction site on the forward primer, and the *HindIII* restriction site on the reverse primer (listed below).

Primer	Primer sequence, 5' to 3'
CyclinA2 EcoRI forwards primer	5' GGC*GAATTC*ATGAATGAAGTACCAGACTAC 3'
CyclinA2 HindIII reverse primer	5' GGC*AAGCTT*TTATTACAGATTTAGTGTCTC 3'
Cdk2 EcoRI forwards primer	5' GGC*GAATTC*ATGGAGAACTTTCAAAAG 3'
Cdk2 HindIII reverse primer	5' GGC*AAGCTT*TTATTAGAGTCGAAGATG 3'

PCR amplification of the CyclinA2 and CDK2 inserts were verified via 1.5% agarose gel electrophoresis, and the samples were extracted and cleaned using the Nucleospin Plasmid Gel and PCR clean-up kit (Takara Bio). PCR reaction mixtures and conditions are listed below.

Component	**Amount (total- 50µL)**
5X Phusion HF (Thermofisher Scientific)	10 µL
dNTPs (10 mM, Thermofisher Scientific)	1 µL
10 µM Forwards Primer	2.5 µL
10 µM Reverse Primer	2.5 µL
Template DNA (~60 ng/µL)	0.5 µL
Phusion DNA Polymerase (2000 units/mL, NEB)	0.5 µL
Autoclaved Water	33 µL

Initial denaturation	98℃, 30 seconds
Cycles- 25X	98℃ for 10 sec, 59.5℃ for 30 sec, 72℃ for 1 min
Final extension	72℃ for 10 minutes

2.1.2. Restriction digestion of PCR product

The CyclinA2 and CDK2 PCR products were digested with *EcoRI* and *HindIII* at 37℃, before the enzymes were inactivated by heating to 80℃ for 30 minutes. Restriction digestion reaction mixture components are listed below.

Component	**Amount (total- 30µL)**
10X cut-smart buffer (NEB)	3 µL
HindIII (20,000 units/mL, NEB)	1.5 µL
EcoRI (20,000 units/mL, NEB)	1.5 µL
PCR product (55 nM)	20 µL
Autoclaved water	4 µL

2.1.3. Restriction digestion of pHMT vector

The pHMT plasmid was isolated using the Nucleospin Plasmid EasyPure mini prep kit (Takara Bio), and digested with *EcoRI* and *HindIII* enzymes. Digestion was verified with 1.5% agarose gel electrophoresis. The restriction digestion reaction mixture for pHMT is listed below.

Component	**Amount (total- 30 µL)**
pHMT vector (50 ng/mL)	23 µL
EcoRI (20,000 units/mL,NEB)	2
HindIII (20,000 units/mL, NEB)	2

10X cut-smart buffer	3

2.1.4. Ligation and transformation

The CyclinA2 and CDK2 gene constructs were ligated into the digested pHMT vector. Ligation products were transformed into electrocompetent *E. coli* DH5α cells. Transformed cells were plated on an LB agar plate with 1 mM carbenicillin and grown overnight at 37℃. Colonies were selected, and the isolated plasmids were submitted for Sanger Sequencing with the forward and reverse primers c verify the presence of the correct target constructs. Absorbance of the digested pHMT plasmids and protein inserts was determined with the Nanodrop Microvolume Spectrophotometer (Thermofisher Scientific) at a wavelength of 260 nm. The Beer-Lambert law was used to extrapolate the concentration. Transformation components are listed below.

Component	**Amount**
Digested pHMT	100 ng
Insert	300 ng
2X electro-ligase buffer (NEB)	11 µL
Electro-ligase (NEB)	2 µL

2.2. Expression of CyclinA2 and CDK2 protein

The CyclinA2 and CDK2 constructs in the pHMT vector were transformed into *E. Coli* BL21-(DE3) cells. Single colonies were picked and grown in 1L of LB or M9 minimal media (66.7 mM Na_2HPO_4, 1.32 mM KH_2PO_4, 18.35 mM $^{15}NH_4Cl$, 0.1 mM $CaCl_2$, 2 mM $MgSO_4$, 10 mL Gibco mix, 22.20 mM Glucose, 1 mL Trace metals mix, and 1 mM Carbenicillin). When grown in M9 minimal media, $^{15}NH_4Cl$ was the sole source of nitrogen for ^{15}N-labeling of the protein for NMR experiments. The cultures were grown at 37℃ until the OD measured between 0.6 and 0.8,

then induced with 1 mM IPTG and grown overnight at 24℃. Following overnight growth, cells were pelleted down by centrifugation (4193 G) and stored at -80℃. Protein expression was verified using SDS-PAGE by visualization with Coomassie blue dye.

2.3. Purification of CyclinA2 protein

For protein purification, cell lysis was performed by sonication in 25 mL of Lysis buffer (50 mM Tris (pH 8), 300 mM NaCl, 10 mM $MgCl_2$, 10 mM TCEP, and 10% glycerol) and 1 cOmplete mini protease inhibitor cocktail tablet (EDTA-free, Millipore sigma). Sonication was performed for 14 minutes, at an amplitude of 50% with 5 seconds on and 2 seconds off in an ice bath. The mixture was then centrifuged for 45 minutes at 2696 G.

The lysate was filtered (1.2µm, Milipore) and the protein was purified over a 5 mL IMAC nickel column (GE Healthcare). The wash buffer (buffer A) consisted of 10 mM Tris (pH 8), 10 mM $MgCl_2$, 25 mM Imidazole, 300 mM NaCl, and 10 mM TCEP. The elution buffer (buffer B) consisted of 10 mM Tris (pH 8), 10 mM $MgCl_2$, 400 mM imidazole, 300 mM NaCl, and 10 mM TCEP. As the MBP-protein constructs included a 6xHis tag, the fusion protein bound to the nickel column in buffer A, before being eluted with a 10 column volume linear imidazole gradient using buffer B. During trials of buffer optimization and CyclinA2 purification, there was a large amount of impurities at each step, and there was evidence of CyclinA2 precipitation following removal of the MBP-6xHis tag construct upon cleavage by TEV protease. Consequently, further purification and complex formation used the MBP-CyclinA2 fusion protein.

Following the first IMAC affinity column, ion-exchange chromatography was performed for further purification. The pooled fractions containing the protein of interest, which were identified using SDS-PAGE and Coomassie blue staining, were dialyzed (10 mM Tris- pH 6.5, 10

mM $MgCl_2$, and 10 mM TCEP), then further purified with a 5 mL Hitrap Q-HP anion exchange column (GE Healthcare). The wash buffer was the same as the dialysis buffer, and the elution buffer consisted of 10 mM Tris (pH 6.5), 10 mM $MgCl_2$, 1 M NaCl, and 10 mM TCEP. After elution, fractions containing the protein of interest were identified using SDS-PAGE gel electrophoresis. As contaminants persisted in the fractions containing CyclinA2, size exclusion chromatography was performed using a Superdex 75 analytical column (Cytiva) in 50 mM Tris (pH 8), 10 mM $MgCl_2$, 150 mM NaCl, and 10 mM BME.

2.4. Purification of unlabeled CDK2

Lysis buffer for unlabeled CDK2 consisted of 50 mM Tris (pH 8), 300 mM NaCl, 10% BME, 0.1% TritonX, and 10% glycerol. 25 mL of Lysis buffer and 1 cOmplete, mini protease inhibitor pellet (EDTA-free, Millipore sigma) were added to a pellet from a 1 L cell culture. Sonication, centrifugation and Nickel column purification steps were identical to CyclinA2 purification. The wash buffer consisted of 50 mM Tris (pH 8), 25 mM Imidazole, 300 mM NaCl, and 10 mM TCEP. The elution buffer consisted of 50 mM Tris, 400 mM Imidazole, 300 mM NaCl, and 10 mM TCEP. The fractions containing MBP-CDK2 were identified with SDS-PAGE Coomassie blue staining, and digested using TEV protease at the cleavage site between CDK2 and MBP. TEV digestion was conducted overnight at room temperature, with a molar ratio of 1:25 for TEV protease to MBP-CDK2. The concentration of the MBP-CDK2 was determined using the Nanodrop Microvolume Spectrophotometer, at a wavelength of 280 nm, and the Beer-Lambert Law (ε = 104,865 M^{-1} cm^{-1}). Overnight dialysis was performed in 1L of the nickel column wash buffer. A second IMAC nickel column was performed with identical buffer conditions as the first, and the flowthrough collected. The presence of CDK2 in the flowthrough was verified using SDS-PAGE and Coomassie staining.

The fractions containing cleaved CDK2 were purified using a 5 mL Hitrap Q-HP column (GE Healthcare). The pooled fractions were dialyzed overnight at 4℃ in 1 L of the Q-Sepharose wash buffer, consisting of 10 mM sodium phosphate (pH 6.6), and 10 mM TCEP. The elution buffer for the anion exchange column consisted of 10 mM sodium phosphate (pH 6.6), 1 M NaCl, and 10 mM TCEP. SDS-PAGE visualization with Coomassie blue staining confirmed the presence of CDK2 in the flowthrough, as well as a single contaminant. To completely purify CDK2, a S75 preparatory size exclusion column was run (Cytiva) in 50 mM Phosphate (pH 8) + 150 mM NaCl + 10 mM TCEP). SDS-PAGE visualization confirmed purification of CDK2.

2.5 Purification of [U- ^{15}N] CDK2

For NMR spectroscopy, ^{15}N CDK2 was expressed in the presence of $^{15}NH_4Cl$ as described in section 2.2. The IMAC columns and TEV cleavage steps in the purification process of ^{15}N-labeled CDK2 were identical to non-labeled CDK2, as detailed in section 2.4. Anion exchange chromatography was performed at an elevated pH of 8.0 (Wash buffer: 10 mM sodium phosphate (pH 8.0), and 10 mM TCEP. Elution buffer: 10 mM sodium phosphate (pH 8.0), 1 M NaCl, and 10 mM TCEP). Following the anion exchange purification, fractions containing purified labeled CDK2 were combined and concentrated with a spin concentrator, until the molarity of the protein reached ~100 µM, measured by the Nanodrop spectrophotometer (Thermofisher Scientific) at 280 nm and the Beer-Lambert Law. Upon concentration, some CDK2 precipitation was observed.

2.6. Formation of CyclinA2 and CDK2 complex

2.6. 1. CyclinA2 and CDK2 complex formation by direct mixing

Multiple methodologies were used to form CyclinA2-CDK2. In the first method, approximately equimolar amounts of purified MBP-A2 and CDK2 were mixed at room

temperature, and then the complex was purified with a Superdex 200 analytical column (Cytivia). The buffer contained 50 mM Tris (pH 8), 10 mM $MgCl_2$, 150 mM NaCl, and 10 mM BME.

2.6.2. CyclinA2-CDK2 complex formation on a Ni^{2+} column

Purified MBP-CyclinA2 was run through a 1 mL IMAC nickel column (GE Healthcare) and allowed to bind to the resin, before being treated with a wash buffer of 10 mM Tris (pH 8), 10 mM $MgCl_2$, 25 mM imidazole, 300 mM NaCl, 10 mM TCEP, and 1 mM ATP. A mixture of cleaved, purified, equimolar CDK2 and 1mM ATP was passed through the column. The column was left for 15 minutes to allow complex formation to occur between MBP-CyclinA2 and CDK2. The protein was eluted with a buffer consisting of 10 mM Tris, 10 mM MgCl2, 400 mM imidazole, 300 mM NaCl, 10 mM TCEP, and 1 mM ATP. The presence of the proteins in fractions were analyzed using SDS-PAGE and Coomassie blue staining. Fractions containing the complex were digested overnight at room temperature with TEV at a ratio of 1:25. The digested complex was then diluted 10x, and run through another IMAC nickel column. The flowthrough was pooled, concentrated, and purified using a Superdex75 analytical gel filtration column (50 mM Tris (pH 8), 10 mM MgCl2, 150 mM NaCl, and 10 mM TCEP). SDS-PAGE visualization was used to determine the presence of the CyclinA2-CDK2 complex, which was confirmed with mass spectrometry.

2.7. SDS-PAGE (protein gel electrophoresis)

SDS-PAGE was used as an analytical tool in detecting protein presence in fractions following purification steps. SDS-PAGE was done using readymade gel and buffer (15% SurePAGE), and visualized with Coomassie blue staining.

2.8. Native Mass Spectrometry

Mass spectrometry can identify a molecule by measuring its molecular weight to a high degree of resolution. The analyte is converted to the gas phase, and an electrical charge is imparted. These charged ions are separated and identified using the mass-to-charge ratio, enabling the calculation of mass and relative abundance of different population states (Urban, 2016). Mass spectrometry was performed by Dr. Sophie Harvey at the CCIC facility, OSU. Samples were dialyzed into a buffer of 200 mM AmAc and analyzed by electrospray ionization on a Q Exactive UHMR instrument (Thermofisher Scientific).

2.9. Nuclear magnetic resonance (NMR) spectroscopy

Purified, [U-^{15}N]-CDK2 was concentrated to approximately 100 µM (approximated due to slight precipitation) and dialyzed into NMR buffer (10 mM sodium phosphate (pH 8), 50 mM NaCl, and 5 mM BME. 10% of D_2O and 1 µL DSS). NMR titrations were performed by Dr. Deepak Kumar Yadav. NMR titrations were performed with ATP and compounds 2-4 (Figure 3). Compounds 2-4 were titrated into CDK2 up to a ratio of approximately 1:2 of the inhibitor to the CDK2 protein (up to 200 µL). As the compounds were dissolved in DMSO, control spectra were collected of free CDK2 and CDK2 in the presence of 2% DMSO.

3. Results

3.1 Subcloning MBP-CyclinA2 and MBP-CDK2 vectors into the pHMT plasmid

Soluble CyclinA2 and CDK2 proved difficult to isolate, therefore both proteins were subcloned into vectors containing an MBP fusion protein. The CyclinA2 and CDK2 PCR

amplification products were visualized with agarose gel electrophoresis, and product band sizes were confirmed with a molecular weight marker, indicating successful amplification (Figure 5A). Following restriction digestion with *EcoRI* and *HindIII,* the samples were used for ligation.

Successful ligation of amplified, restriction enzyme digested CyclinA2 and CDK2 PCR products into pHMT vectors was verified by transformation into *E. coli* DH5α electrocompetent cells, and the growth of colonies on LB agar plates supplemented with carbenicillin (Figure 5B). Sanger sequencing confirmed a 100% match of the CyclinA2 and CDK2 inserts into the pHMT vector (Figure 5C).

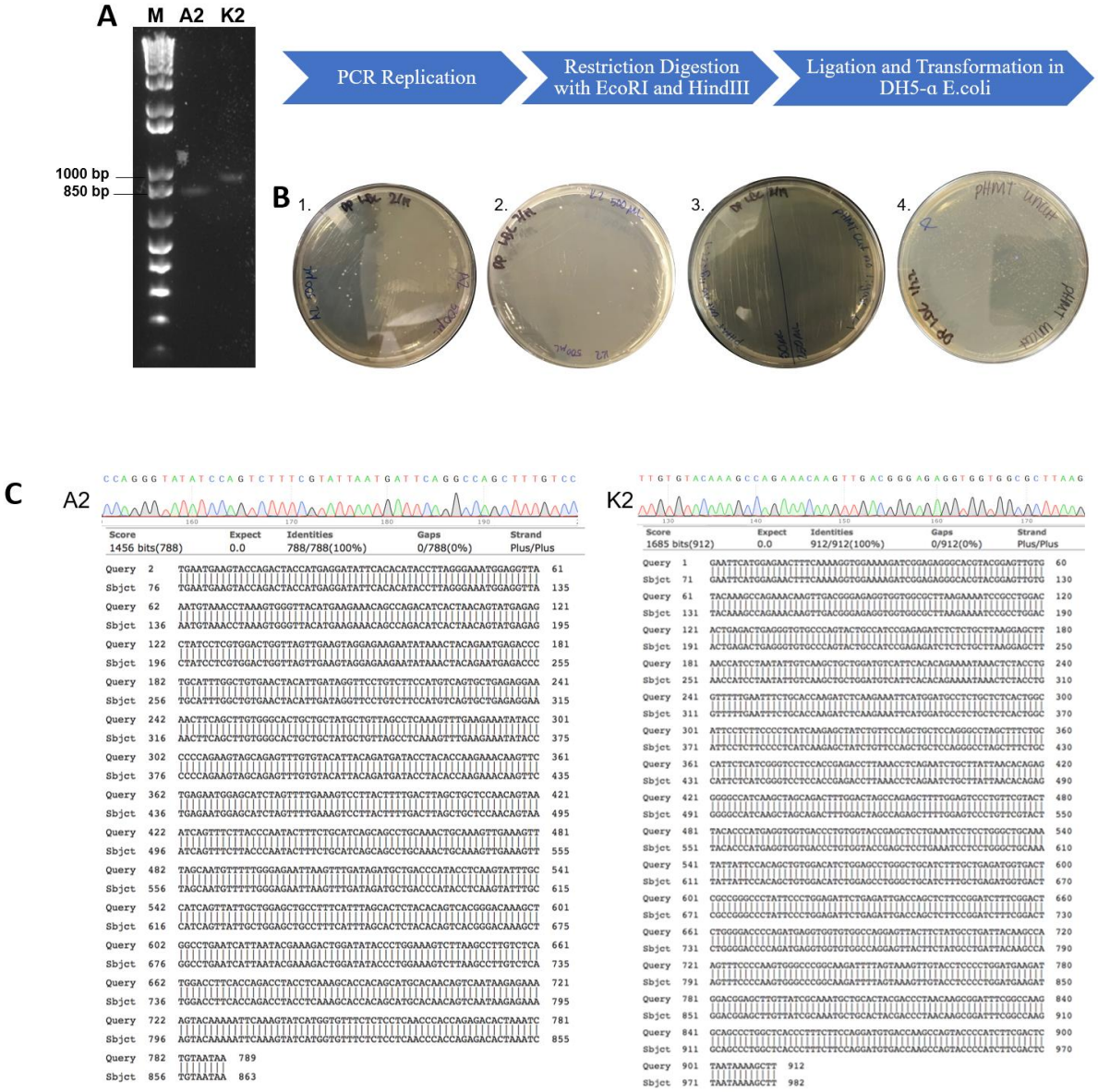

Figure 5: Subcloning and transformation of CyclinA2 and CDK2 **A.** Agarose gel electrophoresis following PCR replication of the CyclinA2 and CDK2 inserts, which indicate PCR amplification product at the expected size. **B.** Colony growth following ligation and electroporation on agar plates with the (1) CyclinA2 insert, (2) CDK2 insert, (3) negative control of cells transformed with the digested vector, (4) and the positive control of cells transformed with the undigested pHMT plasmid. **C.** The chromatograms and sequencing of the transformed colonies indicated

successful subcloning of the CyclinA2 (Left) and CDK2 (Right) inserts, with 100% sequence alignment with the known DNA sequence.

3.2 Protein expression

3.2.1 Expression of MBP-CyclinA2 and MBP-CDK2

MBP-CyclinA2 and MBP-CDK2 were optimally expressed at 24℃. This was visualized with SDS-PAGE and Coomassie blue staining (Figure 6A). Comparison between the induced and uninduced bands of the projected molecular weight following 1 mM IPTG induction showed successful protein expression at the expected molecular weight of 74.30 kDa for MBP-CyclinA2 and 78.26 kDa for MBP-CDK2 (Figure 6B). Uniformly ^{15}N-labeled CDK2 was expressed using minimal M9 media where ^{15}N-ammonium chloride was provided as the sole nitrogen source. When comparing expression in minimal and in LB media, the band intensity of the induced protein was roughly equivalent, and the most intense band corresponded to the molecular weight of the MBP-CDK2 fusion protein (Figure 6C).

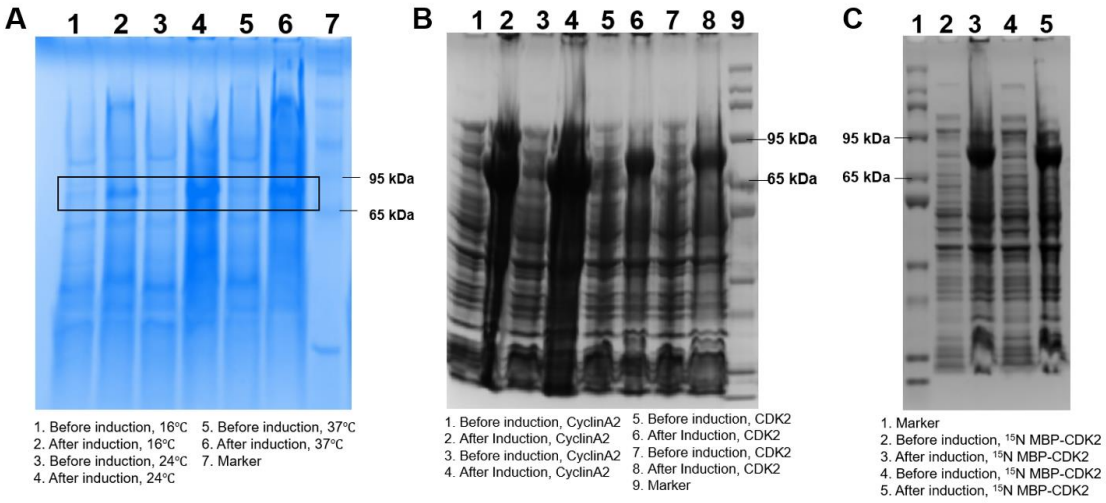

D

	Calculated pI	Calculated Molecular Weight	Amino Acid Sequence
6xHis-MBP-CyclinA2	5.59	74,296.72 Da	MHHHHHHMKI EEGKLVIWIN GDKGYNGLAE VGKKFEKDTG IKVTVEHPDK LEEKFPQVAA TGDGPDIIFW AHDRFGGYAQ SGLLAEITPD KAFQDKLYPF TWDAVRYNGK LIAYPIAVEA LSLIYNKDLL PNPPKTWEEI PALDKELKAK GKSALMFNLQ EPYFTWPLIA ADGGYAFKYE NGKYDIKDVG VDNAGAKAGL TFLVDLIKNK HMNADTDYSI AEAAFNKGET AMTINGPWAW SNIDTSKVNY GVTVLPTFKG QPSKPFVGVL SAGINAASPN KELAKEFLEN YLLTDEGLEA VNKDKPLGAV ALKSYEEELA KDPRIAATME NAQKGEIMPN IPQMSAFWYA VRTAVINAAS GRQTVDEALK DAQTNSSSNN NNNNNNNNLG IEENLYFQGE FMNEVPDYHE DIHTYLREME VKCKPKVGYM KKQPDITNSM RAILVDWLVE VGEEYKLQNE TLHLAVNYID RFLSSMSVLR GKLQLVGTAA MLLASKFEEI YPPEVAEFVY ITDDTYTKKQ VLRMEHLVLK VLTFDLAAPT VNQFLTQYFL HQQPANCKVE SLAMFLGELS LIDADPYLKY LPSVIAGAAF HLALYTVTGQ SWPESLIRKT GYTLESLKPC LMDLHQTYLK APQHAQQSIR EKYKNSKYHG VSLLNPPETL NL
CyclinA2	6.00	30,297.09 Da	GEFMNEVPDY HEDIHTYLRE MEVKCKPKVG YMKKQPDITN SMRAILVDWL VEVGEEYKLQ NETLHLAVNY IDRFLSSMSV LRGKLQLVGT AAMLLASKFE EIYPPEVAEF VYITDDTYTK KQVLRMEHLV LKVLTFDLAA PTVNQFLTQY FLHQQPANCK VESLAMFLGE LSLIDADPYL KYLPSVIAGA AFHLALYTVT GQSWPESLIR KTGYTLESLK PCLMDLHQTY LKAPQHAQQS IREKYKNSKY HGVSLLNPPE TLNL
6xHis-MBP-CDK2	6.13	78,262.51 Da	MHHHHHHMKI EEGKLVIWIN GDKGYNGLAE VGKKFEKDTG IKVTVEHPDK LEEKFPQVAA TGDGPDIIFW AHDRFGGYAQ SGLLAEITPD KAFQDKLYPF TWDAVRYNGK LIAYPIAVEA LSLIYNKDLL PNPPKTWEEI PALDKELKAK GKSALMFNLQ EPYFTWPLIA ADGGYAFKYE NGKYDIKDVG VDNAGAKAGL TFLVDLIKNK HMNADTDYSI AEAAFNKGET AMTINGPWAW SNIDTSKVNY GVTVLPTFKG QPSKPFVGVL SAGINAASPN KELAKEFLEN YLLTDEGLEA VNKDKPLGAV ALKSYEEELA KDPRIAATME NAQKGEIMPN IPQMSAFWYA VRTAVINAAS GRQTVDEALK DAQTNSSSNN NNNNNNNNLG IEENLYFQGE FMENFQKVEK IGEGTYGVVY KARNKLTGEV VALKKIRLDT ETEGVPSTAI REISLLKELN HPNIVKLLDV IHTENKLYLV FEFLHQDLKK FMDASALTGI PLPLIKSYLF QLLQGLAFCH SHRVLHRDLK PQNLLINTEG AIKLADFGLA RAFGVPVRTY THEVVTLWYR APEILLGCKY YSTAVDIWSL GCIFAEMVTR RALFPGDSEI DQLFRIFRTL GTPDEVVWPG VTSMPDYKPS FPKWARQDFS KVVPPLDEDG RSLLSQMLHY DPNKRISAKA ALAHPFFQDV TKPVPHLRL
CDK2	8.61	34,262.88 Da	GEFMENFQKV EKIGEGTYGV VYKARNKLTG EVVALKKIRL DTETEGVPST AIREISLLKE LNHPNIVKLL DVIHTENKLY LVFEFLHQDL KKFMDASALT GIPLPLIKSY LFQLLQGLAF CHSHRVLHRD LKPQNLLINT EGAIKLADFG LARAFGVPVR TYTHEVVTLW YRAPEILLGC KYYSTAVDIW SLGCIFAEMV TRRALFPGDS EIDQLFRIFR TLGTPDEVVW PGVTSMPDYK PSFPKWARQD FSKVVPPLDE DGRSLLSQML HYDPNKRISA KAALAHPFFQ DVTKPVPHLR L
6xHis-MBP	5.32	44,017.65 Da	MHHHHHHMKI EEGKLVIWIN GDKGYNGLAE VGKKFEKDTG IKVTVEHPDK LEEKFPQVAA TGDGPDIIFW AHDRFGGYAQ SGLLAEITPD KAFQDKLYPF TWDAVRYNGK LIAYPIAVEA LSLIYNKDLL PNPPKTWEEI PALDKELKAK GKSALMFNLQ EPYFTWPLIA ADGGYAFKYE NGKYDIKDVG VDNAGAKAGL TFLVDLIKNK HMNADTDYSI AEAAFNKGET AMTINGPWAW SNIDTSKVNY GVTVLPTFKG QPSKPFVGVL SAGINAASPN KELAKEFLEN YLLTDEGLEA VNKDKPLGAV ALKSYEEELA KDPRIAATME NAQKGEIMPN IPQMSAFWYA VRTAVINAAS GRQTVDEALK DAQTNSSSNN NNNNNNNNLG IEENLYFQ

Figure 6: SDS-PAGE gels of MBP-CyclinA2 and MBP-CDK2 expression. **A.** Expression tests of MBP-CyclinA2 at 16℃, 24℃, and 37℃. The most significant difference in band intensity can be seen in the 24℃ trial. **B.** Expression of MBP-CyclinA2 and MBP-CDK2 at 24℃. All 4 pellets show robust expression at the band corresponding to their theoretical mass of 74.3 kDa and 78.3 kDa, respectively. **C.** Expression of ^{15}N MBP-CDK2. Expression of labeled CDK2 is comparable to unlabeled CDK2, and there is robust expression, as indicated by the significant increase in

intensity at the band corresponding to the molecular mass of approximately 79.2 kDa. **D.** Protparam analysis of the MBP-CyclinA2, CyclinA2, MBP-CDK2, CDK2, and 6xHis constructs.

3.3 Protein Purification

3.3.1 MBP-CyclinA2 Purification

Clarified lysate of MBP-CyclinA2 containing the 6xHistag on the MBP fusion protein was applied to an IMAC nickel column. Subsequent SDS-PAGE analysis indicated that a significant percentage of MBP-CyclinA2 had remained in the pellet. Similarly, there is a significant amount of MBP-CyclinA2 present in the flowthrough and wash steps, along with extreme amounts of contamination. The elution step of the affinity column resulted in more pure fractions, with a considerable amount of MBP-CyclinA2. Following anion exchange chromatography, SDS-PAGE revealed that while some impurities were removed, MBP-CyclinA2 still eluted with several contaminants. Between the elution of MBP-CyclinA2 from the IMAC column and further purification using gel filtration chromatography, MBP-CyclinA2 underwent degradation. Consequently, the size exclusion column load had an increase in impurities, particularly the concentration of the impurity weighing approximately 50 kDa, (Figure 7B Lane L). The SDS-PAGE gel showed MBP-CyclinA2 to elute in peak 1, at 8.73 mL and slightly in peak 2, at 12.31 mL (Figure 7B). Using a calibration curve derived from standards of known molecular weight, it became clear that the fusion protein was eluting at an apparent mass of 422.9 kDa and 143.4 kDa, as opposed to its theoretical mass of 72.3 kDa. This indicated dimeric and hexameric oligomer states existed in solution (Figure 7A), and overall yield of MBP-CyclinA2 was low.

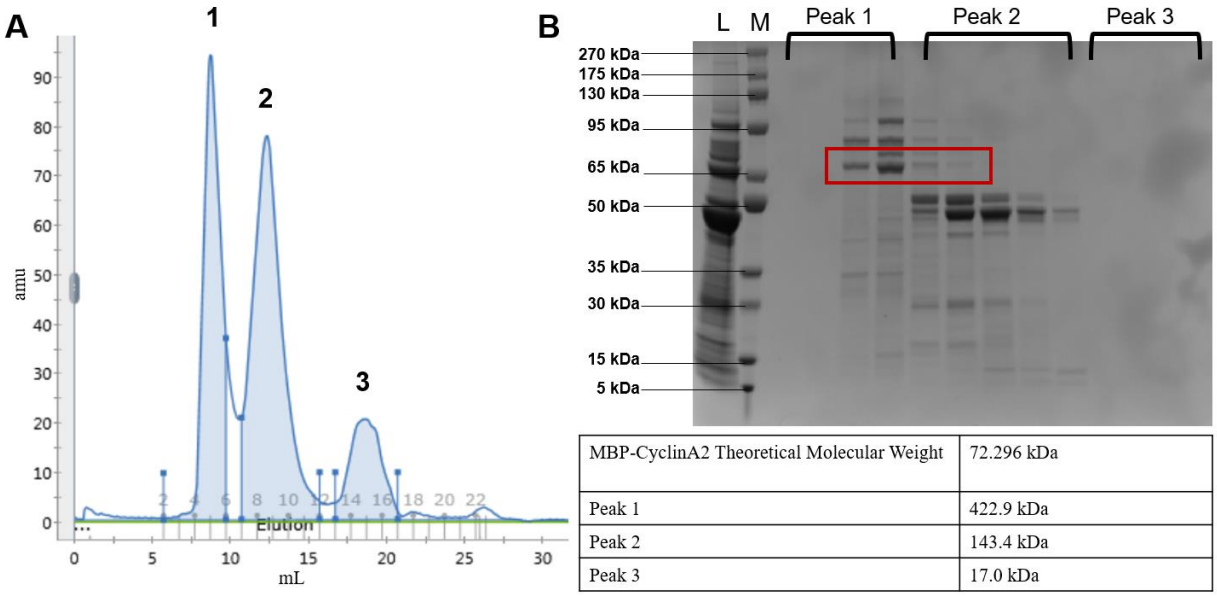

MBP-CyclinA2 Theoretical Molecular Weight	72.296 kDa
Peak 1	422.9 kDa
Peak 2	143.4 kDa
Peak 3	17.0 kDa

Figure 7: Oligomerization of MBP-CyclinA2. **A.** The chromatogram (280 nm) from an S75a size exclusion column showed three eluted peaks. The calculated molecular weights of each elution volume are listed in the Table above. **B.** SDS-PAGE shows a band corresponding to the theoretical size of MBP-CyclinA2 eluting in both peaks 1 and 2 (red box).

3.3.2 Purification of Unlabeled CDK2

The purification of MBP-CDK2 was successful and did not present the degradation problems which had persisted with MBP-CyclinA2. Analysis of the first IMAC nickel column with SDS-PAGE did not show a significant amount of MBP-CDK2 in the pellet, and the impurity of the sample caused difficulty when characterizing the relative amount of CDK2 in the lysate, flowthrough, and wash. While the elution step with high imidazole removed a significant portion of impurities compared to the purification of MBP-CyclinA2, there were still several contaminants present. TEV digestion was performed to remove the MBP-6xHis tag construct. Following

digestion, the sample was loaded and eluted from a second IMAC nickel column. SDS-PAGE analysis of the peak fractions showed CDK2 in the flowthrough, where it was expected to fractionate, and an additional peak during the linear imidazole gradient elution phase containing MBP, other contaminants, and the TEV protease. There was clear separation of most of the MBP folding chaperone from CDK2. However, several contaminants were still present, including a faint band at the molecular weight corresponding to MBP. These were present in far less quantities than CDK2. The anion-exchange column chromatogram indicated a plateaued peak where CDK2 eluted in the flowthrough, and a collection of peaks where MBP and other contaminants fractionated during the elution phase. SDS-PAGE analysis indicates almost complete purification of CDK2, except for a faint impurity corresponding to the molecular weight of the 6xHis-MBP construct.

Prior to gel filtration chromatography, concentration of the pooled CDK2 fractions caused some precipitation (Figure 8, lane L). This final step partially separated CDK2 from the impurity, allowing for further analysis of both populations. Both CDK2 and the MBP contaminant, with theoretical molecular weights of 34.26 kDa and 44.02 kDa respectively, eluted under the same, symmetrical peak (Figure 8).

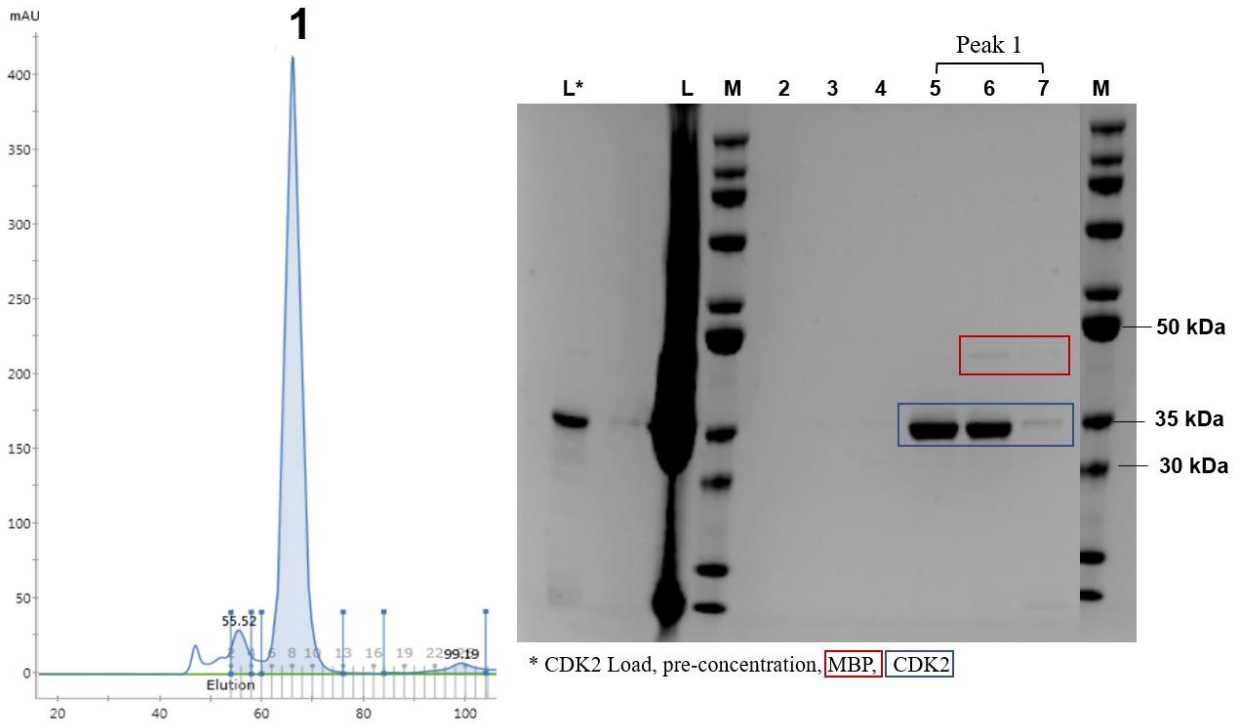

Figure 8: Final purification step of CDK2. The S75p chromatogram (280 nm) shows a singular, symmetric peak, in which both the CDK2 (blue square, 34 kDa) and MBP (red square, 44 kDa) contaminant eluted. The SDS-PAGE gel confirms this, and the MBP contaminant is only present in fractions 6 and 7.

3.3.3 Purification on [U-^{15}N]- CDK2

Purification of ^{15}N-CDK2 followed similar trends as the purification of the unlabeled protein. The chromatogram from the first nickel column showed a large peak eluting with the application of the high-imidazole buffer gradient. SDS-PAGE confirmed the peak to contain CDK2, however, there was a significant amount of CDK2 in the flowthrough and wash potentially due to overloading of the column. These fractions were pooled and run through an additional IMAC column, with the lower imidazole concentration in the loading buffer further separating the

contaminants in the wash and flowthrough from the protein, which bound to the column. SDS PAGE showed that more CDK2 had separated from the other impurities and could be pooled with the relevant fractions from the first nickel column. TEV protease was added to the fractions at a 1:25 ratio, which cleaved almost all the MBP from CDK2. The ratio of 1:25 was chosen as trials with less TEV resulted in a large amount of un-cleaved fusion protein remaining following overnight digestion.

The chromatogram from the anion exchange column showed a sustained plateau for the flowthrough, where CDK2 was expected to elute. A peak containing the remainder of the contaminants, including the MBP construct, eluted at a high concentration of NaCl (Figure 9, Lane E). Interestingly, the anion exchange chromatography step for the labeled protein, at a buffer of pH 8, was much more efficient in completely purifying CDK2 compared to the anion exchange column used in unlabeled CDK2 purification, performed at a pH of 6.6. Spin concentration was required and throughout the concentrating process CDK2 slightly precipitated, resulting in a white hue to the solution. The concentration was determined using the Beer-Lambert law and the absorption at 280 nm.

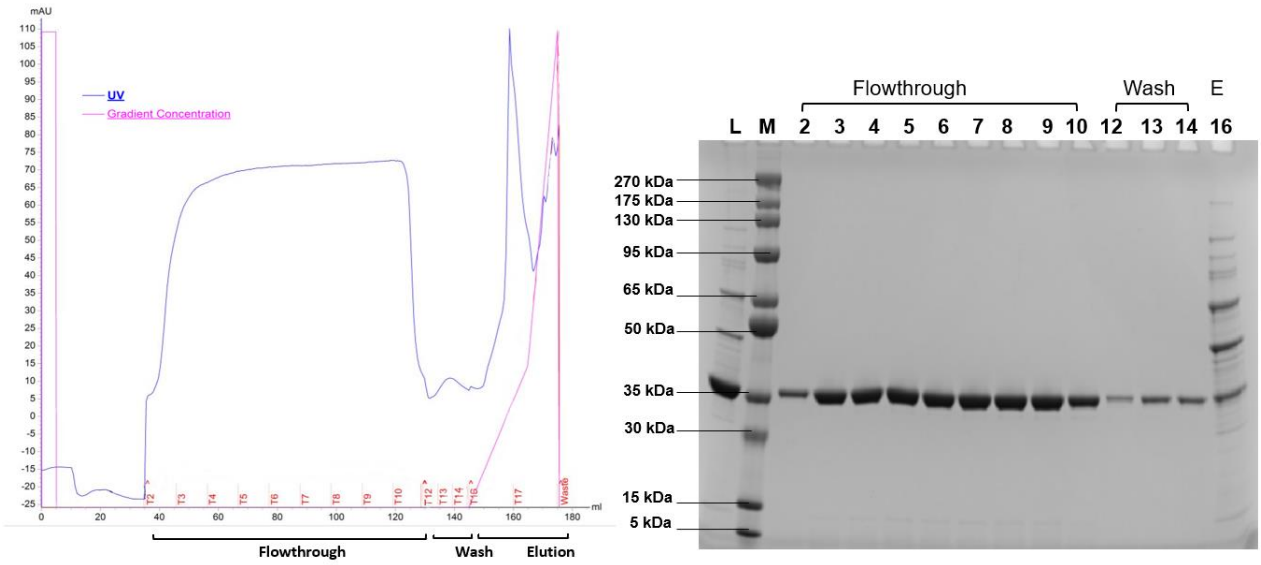

Figure 9: Final purification step of ^{15}N CDK2. Anion exchange chromatography was the final step in purifying ^{15}N CDK2. The chromatogram shows a sustained plateau during the loading step, in which the pure CDK2 is collected in the flowthrough. A large peak at the elution step of the chromatogram, and the right-most lane on the SDS-PAGE gel, corresponds to the elution of the MBP construct, as well as all other contaminants.

3.4 Complex formation

3.4.1. Complex Formation by Mixing

The mixing of CDK2 and MBP-CyclinA2 did not form a singular complex, as evident by the elution of two distinct peaks on a size exclusion column, one of which corresponding to approximately 39 kDa, and the other corresponding to approximately 622 kDa (Figure 10).

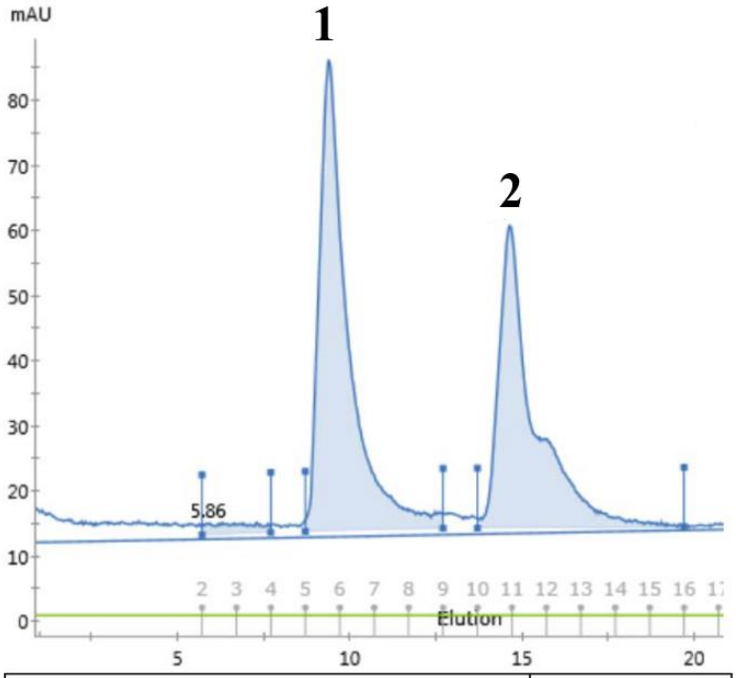

Peak 1	672.6 kDa
Peak 2	39.8 kDa
Calculated Mass of MBP-CyclinA2	74.3 kDa
Calculated mass of CDK2	34.3 kDa
Calculated Mass of the MBP-CyclinA2 CDK2 complex	108.6 kDa

Figure 10: Gel filtration of mixing CDK2 and MBP-CyclinA2. Mixing equimolar amounts of CDK2 and MBP-CyclinA2 prior to purification with size exclusion chromatography resulted in the elution of 2 distinct peaks, neither of which corresponded to the calculated molecular weight of the complex.

3.4.2. Complex Formation by Nickel column

Complex formation in a nickel column was attempted by allowing MBP-CyclinA2 to bind to the resin, then adding CDK2. Binding would occur within the column, and the complex would

elute in the same fraction with the application of the elution buffer. An SDS-PAGE gel was run following the complex formation by nickel column. The MBP-CyclinA2 load can be seen to have multiple contaminants (Figure 11A, lane 1), while the CDK2 loads are almost devoid of impurities (Figure 11A, Lane 2). A band corresponding to CDK2 can be seen in the flowthrough fractions (Figure 11A, Lane 5). However, this is a much fainter band than the initial load. MBP-CyclinA2, CDK2, and several impurities eluted in the same fraction, indicating that they eluted simultaneously (Figure 11A, lane 6). Following TEV digestion, and a second nickel column purification, SDS-PAGE displayed both bands corresponding to the CyclinA2 and CDK2 proteins in the flowthrough (Figure 11B, Lane 3). In the same elution fraction as MBP, there is still an amount of undigested MBP-CyclinA2. Concentration of the flowthrough yielded a fraction with one major contaminant, which was removed using size exclusion chromatography, and the purity was confirmed with SDS-PAGE gel electrophoresis (Figure 11C). Native mass spectrometry identified a species with an experimentally determined mass that was similar to the theoretical mass of the CyclinA2-ATP-CDK2 complex, suggesting successful complex formation (Figure 11D).

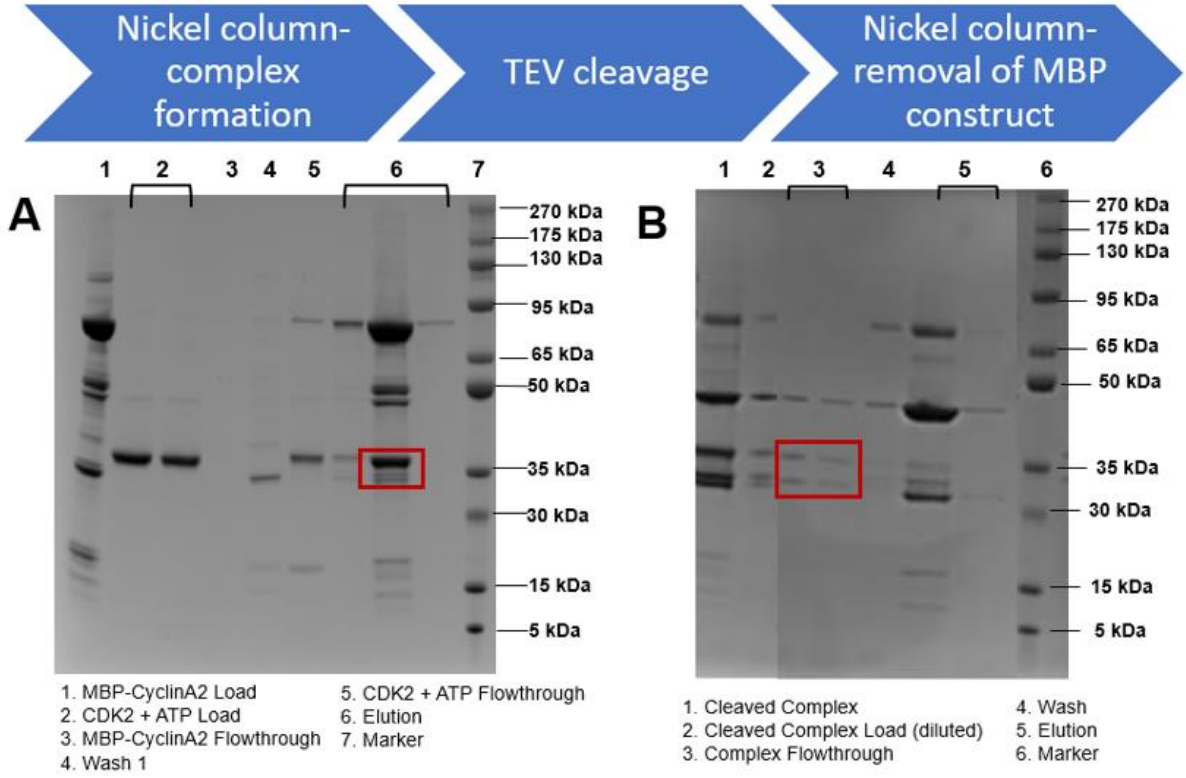

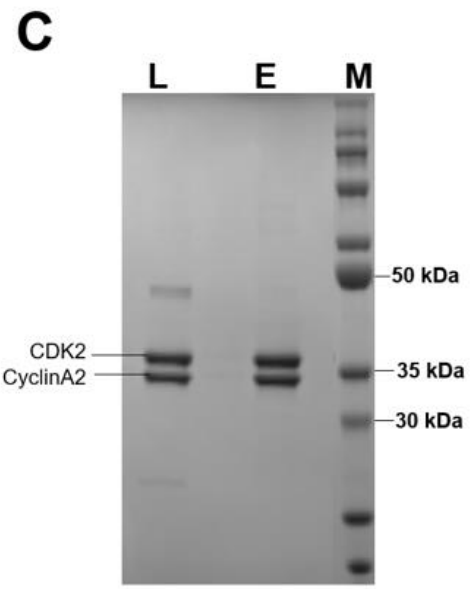

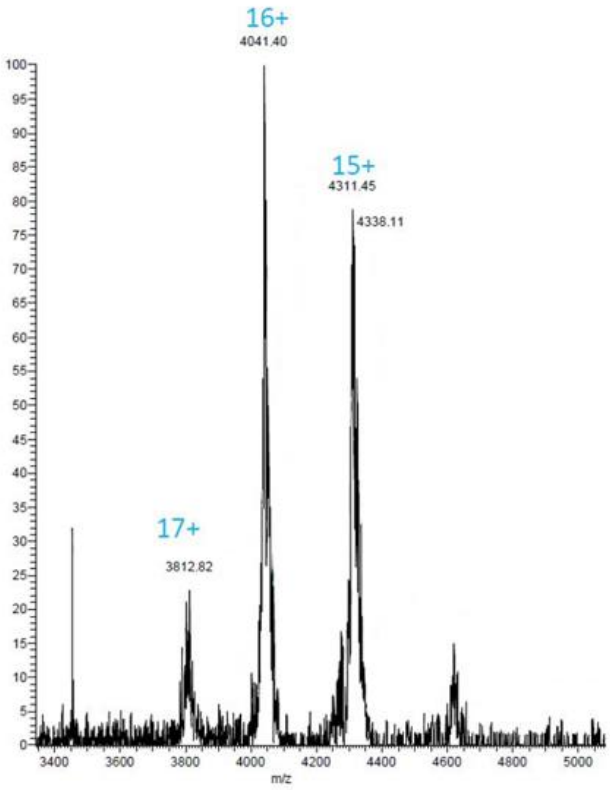

Experimental Molecular Weight:	64,780 ± 6 Da
Theoretical Molecular Weight:	65,065 Da

Figure 11: Formation of the CyclinA2-CDK2 complex. **A.** The SDS-PAGE gel for the first nickel column fractions, with the steps associated with each lane listed below. The presence of the band corresponding to the molecular weight of CDK2 in the same elution step as MBP-CyclinA2 indicates complex formation (red square). **B.** SDS-PAGE gel following TEV digestion and removal of the MBP construct. The steps corresponding to each lane are listed below. There is evidence of CyclinA2 and CDK2 in the flowthrough (red square). **C.** SDS-PAGE of the size exclusion run. The load (L), elution (E), and pre-stained marker (M) are labeled. **D.** Native mass spectrometry yields signals corresponding to the CyclinA2-CDK2 complex.

3.4.3 Native Mass Spectrometry of CDK2

Native mass spectrometry was conducted on unlabeled and ^{15}N-labeled CDK2 to verify the identity of the purified protein by size. Native mass spectrometry revealed multiple population states of CDK2 in both ^{15}N labeled and unlabeled samples. Peaks were identified which corresponded to the mass of unbound CDK2, phosphorylated CDK2, CDK2 bound to adenosine, and phosphorylated CDK2 bound to adenosine. With the addition of ATP, the same four states persisted, and there were no additional peaks identified corresponding to the molecular weight of CDK2 bound with ATP (Figure 12).

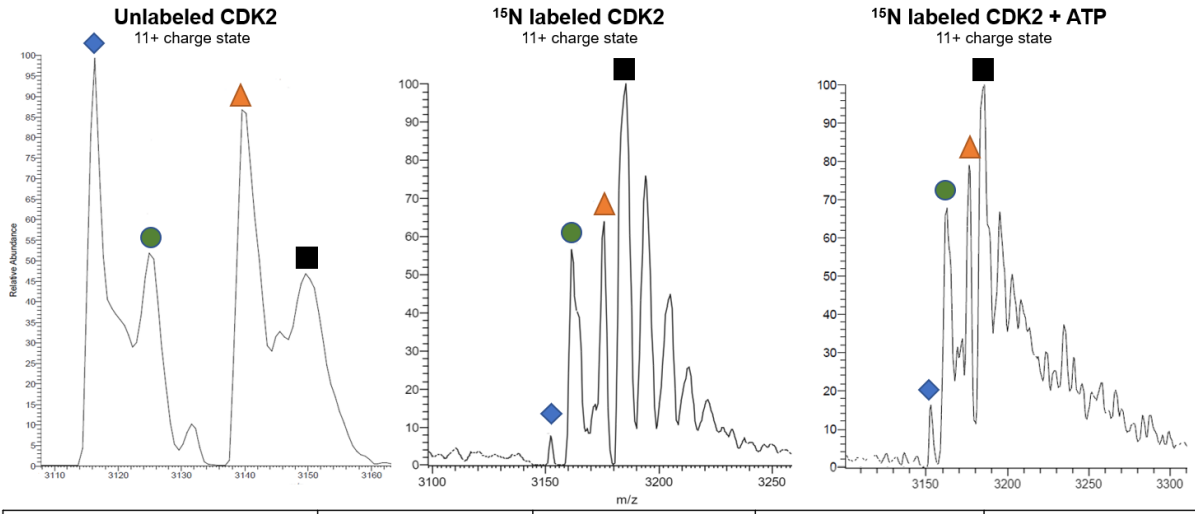

	CDK2 predicted mass	CDK2 experimental mass	^{15}N CDK2 predicted mass	^{15}N CDK2 experimental mass
CDK2 ◆	34,263 Da	34,269 ± 2 Da	34,674 Da	34,668 ± 1 Da
Phosphorylated CDK2 ●	34,343 Da	34,365 ± 1 Da	34,754 Da	34,775 ± 5 Da
CDK2 + adenosine ▲	34, 530 Da	34,528 ± 2 Da	34,941 Da	34,924 ± 2 Da
Phosphorylated CDK2 + adenosine ■	34, 610 Da	34,637 ± 2 Da	35,021 Da	35,030 ± 2 Da

Figure 12: Mass spectrometry revealed multiple population of CDK2. In both unlabeled and ^{15}N-labeled CDK2, four population states were observed, most clearly visualized at the 11+ charge state.

3.4.4 NMR spectroscopy

Purified [U-^{15}N]-CDK2 was concentrated up to 100 µM, and slight precipitate was noted in the sample, as evident by a milky white layer in the bottom of solution. This made exact quantification of CDK2 concentration impossible, but approximately 100 µM CDK2 was used for each titration.

Due to the absence of published backbone chemical shift assignments of CDK2, ^{15}N-HSQC peaks could not be assigned to their respective residues. However, general observations can be made about the free CDK2 protein based on the quality of the ^{15}N-HSQC spectrum (Figure 13A).

Most of the peaks look well resolved and distributed across the spectrum, indicating a well folded CDK2 protein. Using this spectrum as a reference, qualitative observations were made about interactions between CDK2 and the compounds, as well as ATP.

To ensure that the presence of DMSO was note responsible for the observed changes in the spectrum, a control experiment of CDK2 in the presence of 2% DMSO was recorded. An overlay of the spectra of CDK2 and CDK2+ DMSO shows almost identical amide proton chemical shifts (Figure 13B)

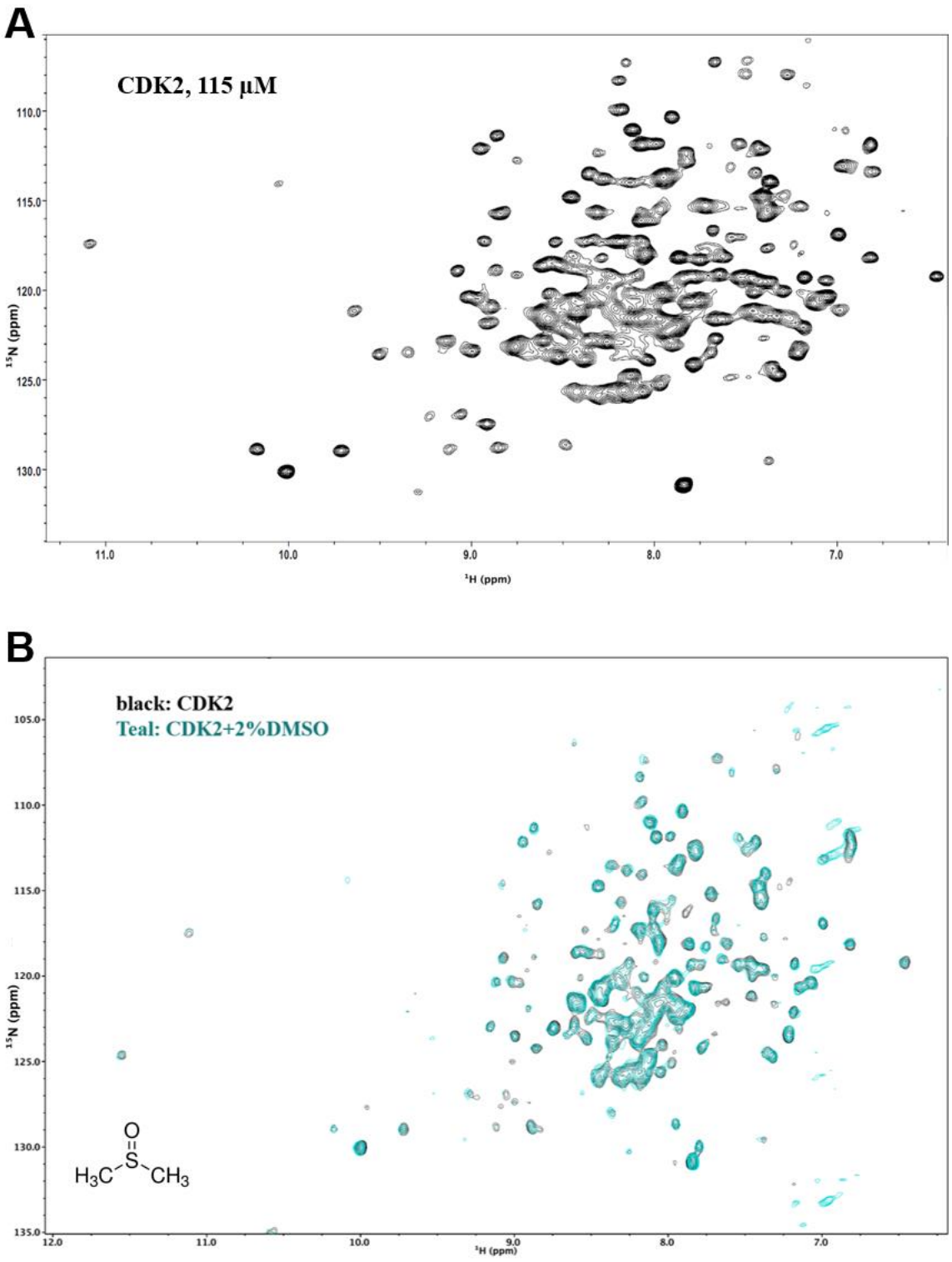

Figure 13: HSQC Titration Controls: **A.** HSQC spectrum of CDK2. The spectrum looks well resolved, and the protein appears to be folded. **B.** DMSO control. Overlaying the spectrum of free

CDK2 and CDK2 + 2% DMSO does not show significant CSP, indicating that it will not be a confounding variable.

Addition of higher concentrations of ATP (200 µM and 1 mM) in the presence of magnesium resulted in significant increases in chemical shift perturbations (Figure 14).

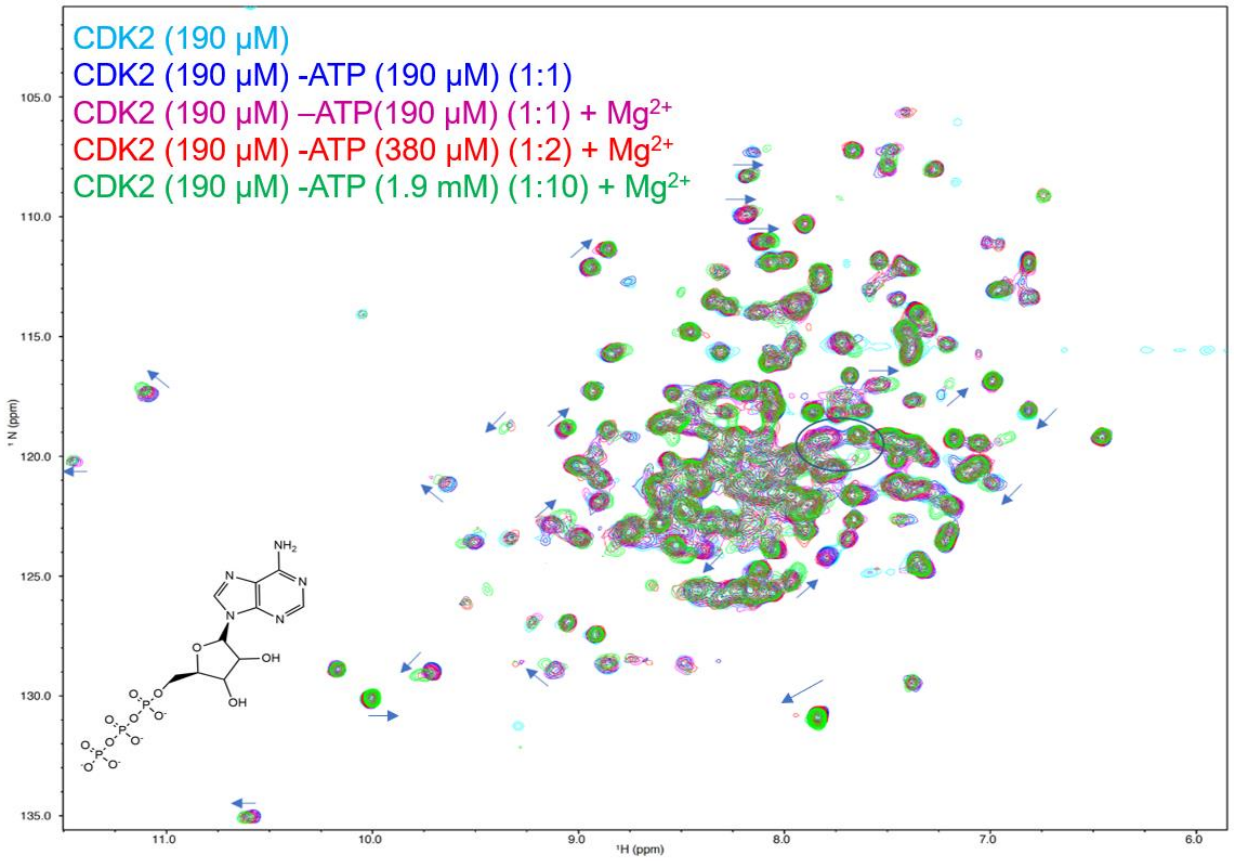

Figure 14: titration of CDK2 with ATP in the presence of magnesium. The ^{15}N-HSQC spectra of free CDK2 (190 µM), CDK2 + ATP (190 µM), CDK2 + Mg^{2+} (190 µM) + ATP (190 µM), CDK2 + Mg^{2+} (190 µM) + ATP (380 µM), and CDK2 + Mg^{2+} (190 µM) + ATP (1.9 mM) are overlayed.

Peaks with significant chemical shift perturbations are marked with an arrow, pointing in the direction of the shifts from free CDK2 to ATP bound CDK2.

The Titration with Compound 2: In comparison to the other inhibitors and ATP, compound 2 was observed to have the largest impact in chemical shift perturbations. These chemical shift perturbations progress in a step-wise fashion as the concentration of the compound increased to 200 μM (Figure 15A). However, addition of magnesium did not lead to any significant CSP (Figure 15B), which indicates that magnesium is not required for interaction between compound 2 and CDK2.

Titration of Compound 3: Stepwise chemical shift perturbations can be seen with throughout the compound 3 titration with CDK2. Similar to compound 2, backbone CSP of the CDK2 protein with addition of compound 3 indicates that the protein interacts with the inhibitor (Figure 15C). The addition of magnesium produced similar results to the trial with compound 2 and did not cause additional peak shifting. This indicated that CDK2 does not require magnesium as a prerequisite for binding to compound 3.

Titration of Compound 4: The titration of compound 4 into CDK2 caused progressive chemical shift perturbations, similar to compounds 2 and 3 (Figure 15D). CSPs in the HSQC titration spectrum with CDK2 in the presence of compound 4 indicates that the protein interacts with the ligand.

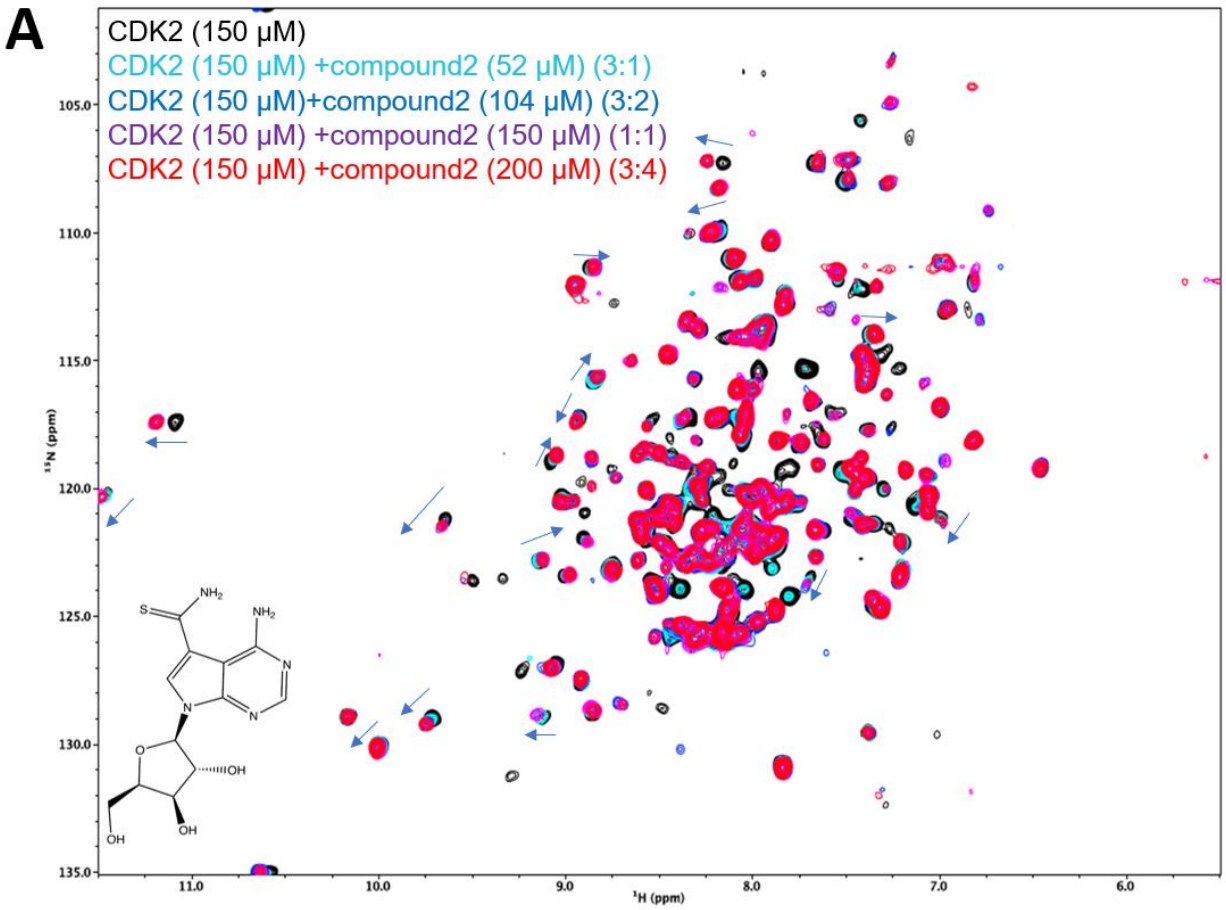
A
CDK2 (150 μM)
CDK2 (150 μM) +compound2 (52 μM) (3:1)
CDK2 (150 μM)+compound2 (104 μM) (3:2)
CDK2 (150 μM) +compound2 (150 μM) (1:1)
CDK2 (150 μM) +compound2 (200 μM) (3:4)
105.0
110.0
115.0
120.0
125.0
130.0
135.0
^{15}N (ppm)
11.0
10.0
9.0
8.0
7.0
6.0
^{1}H (ppm)
NH2
NH2
S
N
N
N
O
OH
OH
OH

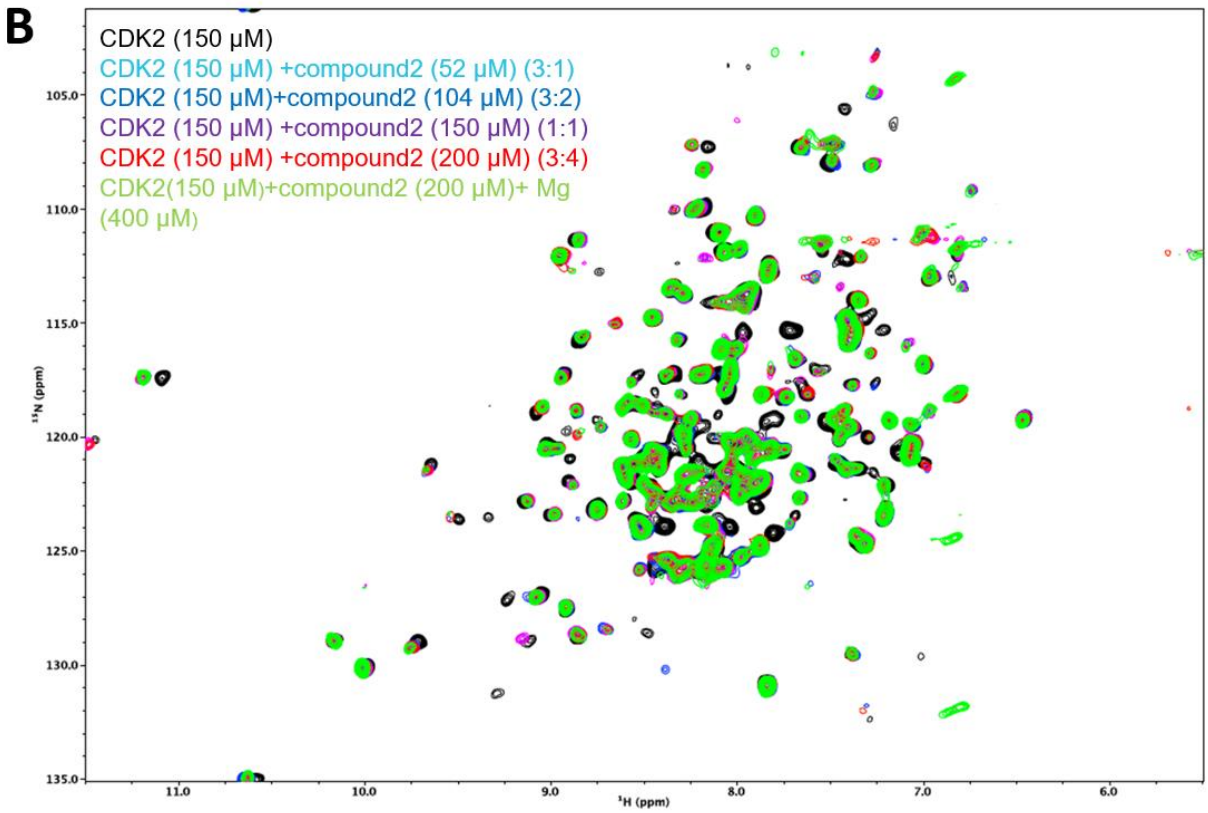
B
CDK2 (150 μM)
CDK2 (150 μM) +compound2 (52 μM) (3:1)
CDK2 (150 μM)+compound2 (104 μM) (3:2)
CDK2 (150 μM) +compound2 (150 μM) (1:1)
CDK2 (150 μM) +compound2 (200 μM) (3:4)
CDK2(150 μM)+compound2 (200 μM)+ Mg (400 μM)
105.0
110.0
115.0
120.0
125.0
130.0
135.0
¹⁵N (ppm)
11.0
10.0
9.0
8.0
7.0
6.0
¹H (ppm)

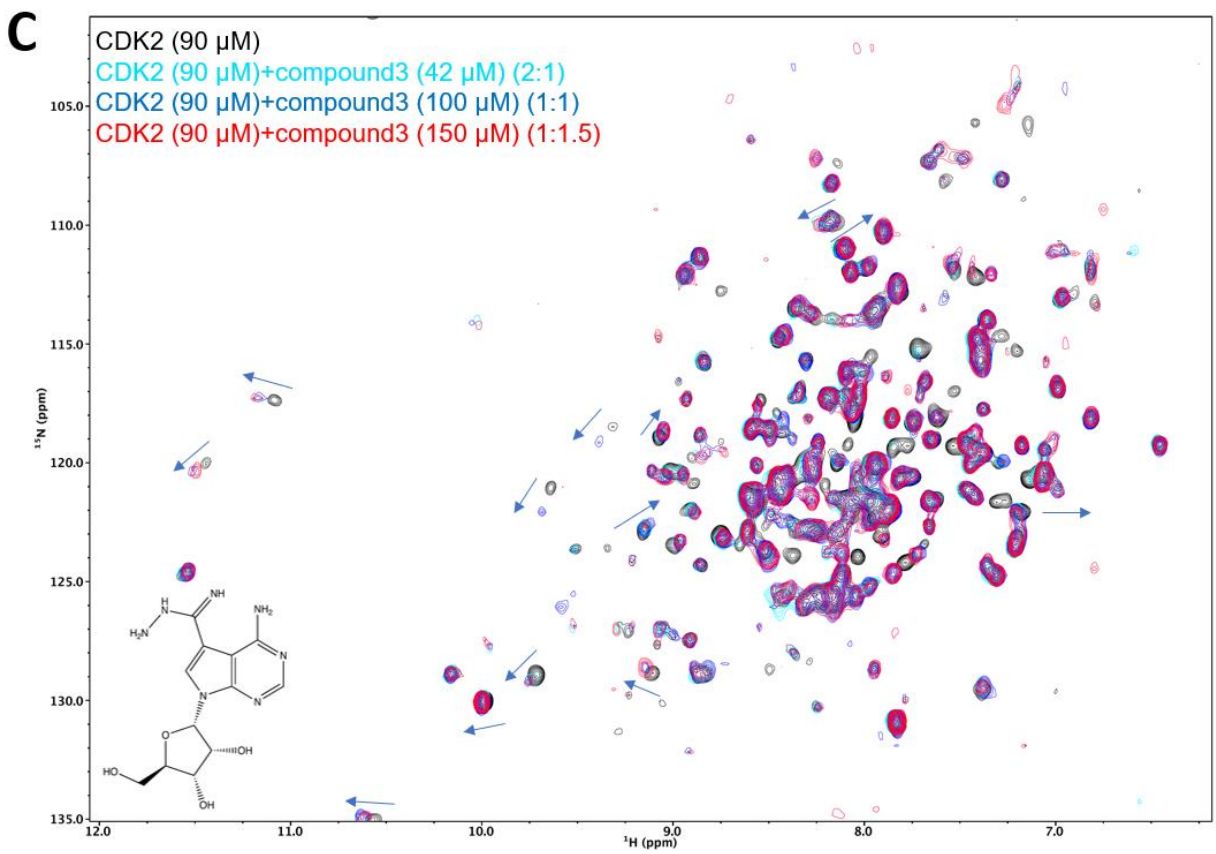
C
CDK2 (90 μM)
CDK2 (90 μM)+compound3 (42 μM) (2:1)
CDK2 (90 μM)+compound3 (100 μM) (1:1)
CDK2 (90 μM)+compound3 (150 μM) (1:1.5)
105.0
110.0
115.0
120.0
125.0
130.0
135.0
15N (ppm)
12.0
11.0
10.0
9.0
8.0
7.0
1H (ppm)
NH
NH2
H2N
N
N
O
OH
HO
OH

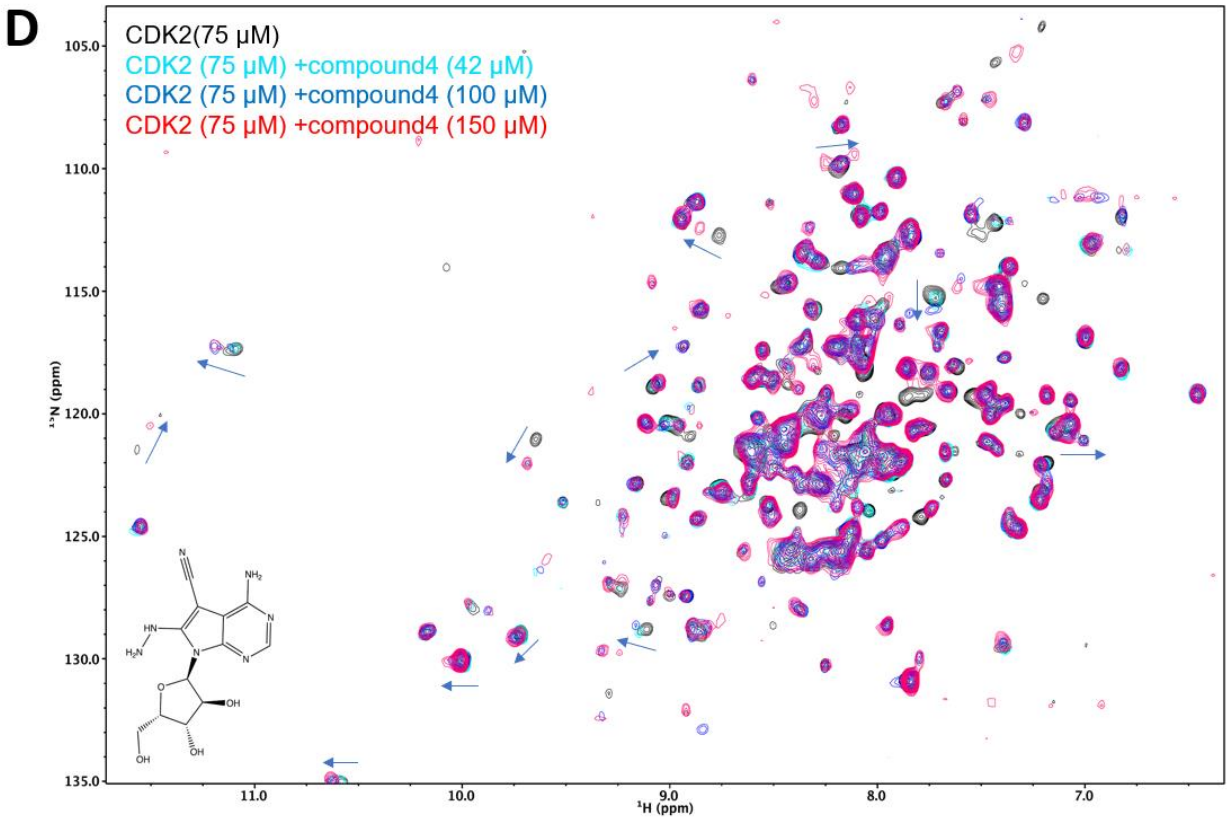

Figure 15: NMR spectra of CDK2 in absence and presence of varying concentrations of ligand. **A**. Titration of compound 2 into CDK2. The spectra of free CDK2 (150 µM), and CDK2 + compound 2 at concentrations of 52 µM, 104 µM, 150 µM, and 200 µM are overlayed. **B**. The spectra pictured in figure 15A is overlayed with the spectra of CDK2 + compound 2 (200µM) + Mg^{2+} (400µM) There is not a significant amount of additional chemical shift perturbations. Addition of magnesium to the CDK2 + compound 3 titration similarly resulted in few CSP. **C**. Titration of compound 3 into CDK2. The spectra of free CDK2 (90 µM), CDK2 + compound 3 at concentrations of 42 µM, 100 µM, and 150 µM are overlayed. **D**. Titration of compound 4 into CDK2. The spectra of free CDK2 (75 µM, CDK2 + compound 4 at concentrations of 42 µM, 100 µM, and 150 µM are overlayed. In **A**, **C,** and **D**, peaks with significant chemical shift perturbations

are marked with an arrow, pointing in the direction of the chemical shift from free CDK2 to CDK2 bound to each compound.

4. Discussion

4.1 Expression and purification of proteins

The decision to include MBP as a fusion protein stemmed from its ability to increase solubility and therefore yield of protein, the mechanism of which is predicted to be by passively inhibiting aggregation pathways (Waugh, 2016). The aggregation of CyclinA2 is characteristic of some eukaryotic proteins, which may form insoluble inclusion bodies when expressed in *E. coli*. Prokaryotic cellular conditions are different than eukaryotic, and the prokaryotic cell cannot complete necessary post-translational modifications, potentially resulting in an incomplete or mis-folded protein.

While SDS-PAGE is a powerful tool in determining the presence and relative purity of the target protein, the reducing agent present in the loading dye dissolved the MBP-CyclinA2 soluble aggregates by reducing cysteine-cysteine bonds. Consequently, throughout purification steps, it appeared that MBP-CyclinA2 was monomeric in solution. However, size exclusion, which allows visualization of the molecular weight in native conditions, showed oligomerization of MBP-CyclinA2 into approximately a hexamer and a dimer. MBP-CyclinA2 seemed to undergo degradation, even when stored at 4℃. The degradation of MBP-CyclinA2, paired with the poor yield due to instability of CyclinA2, presented substantial difficulties in purification.

In the purification of both labeled and unlabeled CDK2, the 6xHis-MBP contaminant persisted, however it was present in a higher relative concentration with the ^{15}N labeled CDK2.

This presented difficulties in purifying a sample enough to conduct NMR. Theoretically, as the fusion protein had bound to the nickel-coated resin in the initial affinity column, the cleaved 6xHis-MBP construct should have bound to the second affinity column as well. Potential causes as to the presence of the impurity in the flowthrough include interactions between the cleaved MBP construct and CDK2 following the TEV treatment. In size exclusion chromatography, the MBP contaminant persisted. This is not unsurprising, as the size difference between the construct and CDK2 is only roughly 10 kDa. There is a small degree of separation, however, as the MBP contaminant eluted in the second collected fraction only. Interestingly enough, the general pattern of size exclusion chromatography dictates that an increase in elution volume corresponds to a decrease in molecular weight, suggesting that the MBP construct behaved as a protein with a smaller molecular weight than CDK2. Potential reasons for this discrepancy could be the shape of MBP, affecting intercalation through the resin. If MBP was globular or compact enough, it might behave as a smaller protein. Opposingly, CDK2's bi-lobar structure could have caused it to behave as a larger protein.

For CDK2 purification, anion exchange chromatography was used to remove the MBP impurity. The theoretical pIs of CDK2 and the MBP construct are 8.61 and 5.32, respectively. Therefore, the first anion exchange purification step was completed at pH 6.6, with the expectation that the MBP construct would interact with the positively charged resin, while CDK2 would elute in the flowthrough. Puzzlingly, following this step there was still the MBP contaminant present in the sample. For the ^{15}N labeled CDK2 purification, anion exchange chromatography was performed at pH 8.0, in attempt to maximize MBP binding to the column. In these conditions, separation of the MBP contaminant was absolute. This implies that the theoretical pI of the MBP

construct may not have been accurate in the presence of CDK2, as it behaved like a protein with a more elevated pI.

4.2 Native Mass Spectrometry of CDK2

Native mass spectrometry showed the same four population states for both ^{15}N-labeled and unlabeled CDK2, and in varying conditions of magnesium and ATP. There is a conserved phosphorylation point on CDK2 at Thr160, which must be phosphorylated following CyclinA2 binding for activation of the complex. However, this phosphorylation site is usually buried until the CDK has undergone the conformational change associated with Cyclin binding. Phosphorylation could still occur, as there are additional inhibitory phosphorylation sites on CDK2, and some evidence that the activation loop containing the phosphorylation site at Thr160 may be flexible enough to allow for phosphorylation before Cyclin binding (Desai, et al. 1995). The molecular weight of the third and fourth CDK2 population states correspond to CDK2 and phosphorylated CDK2 bound to adenosine. Since CDK2 binds ATP, the ligand binding site could facilitate a lone adenosine base. Additionally, efforts to dislodge adenosine by repeating the mass spectrometry with a 1:1 ratio of CDK2 and ATP in the presence of magnesium did not result in the expected corresponding peaks. A potential reason for this is the sample is dialyzed into a buffer of 200 mM AmAc just before collecting native mass spectrometry data. It is possible that the ATP was dialyzed out of the sample. Further trials with the addition of ATP and magnesium after dialysis are required to fully understand the behavior of CDK2 binding to ATP.

For all three samples, while the population states are all present, they are different in their relative abundance. In both ^{15}N spectra, the phosphorylated states decreased in relative abundance, and the adenosine-bound states increased in abundance.

4.7 HSQC NMR of CDK2

Compounds 1, 2, 3, and 4 dissolved in 100% DMSO were received from Dr. Jose Otero's lab. DMSO, an organic solvent, is necessary to dissolve nonpolar organic compounds, but can cause denaturation of proteins at a high concentrations (Abraham et al., 2006). Consequently, the presence of DMSO at higher concentrations can cause chemical shift perturbations in ^{15}N-HSQC NMR experiments. To minimize the effect of DMSO on protein folding and stability, ^{15}N-HSQC NMR experiments were performed in the presence of 2% DMSO. As the overlay of the spectra shows minimal CSP, the presence of DMSO in the buffer can be disregarded as a potential confounding variable.

Chemical shift perturbations of CDK2 increased in magnitude with a higher concentration of ATP and in the presence of magnesium. This indicates that magnesium may be required for ATP binding, and is supported by literature (Bao et al., 2011). The noticeable CSP in ^{15}N-HSQC NMR experiments are present even with a 3:1 ratio of CDK2 to compound 2. This indicates that CDK2 is binding with stronger affinity relative to ATP. Furthermore, these step-wise shifts occur prior to the addition of magnesium, and the addition of magnesium does not cause any additional CSP. This suggests that, unlike ATP, CDK2 may not require magnesium to bind to compound 2.

Similarly, significant CSPs are observed in ^{15}N-HSQC NMR experiments of CDK2 titrations with compound 3 in absence of magnesium.

Interestingly, the comparison of the CDK2 titrations with ATP and the different compounds showed some similarities. While the direction and magnitude of the chemical shifts varied from spectrum to spectrum, the identity of many of the peaks affected was uniform (Figure 16C). This indicates that ATP and the compounds interacted with CDK2 in a similar fashion, at the ATP binding cleft. This is somewhat unsurprising, as the structures of the compounds are similar to ATP, including a carbohydrate moiety and the linked 5 and 6 atom rings that are structurally similar to adenosine (Figure 16B). In addition, it appears that by comparing ^{15}N-HSQC of CDK2 at concentrations of 200 µM for the compounds and 1 mM for ATP, the magnitude of the amide peak shift was on average much greater in presence of the compounds (Figure 16A). This suggests that CDK2 has a greater affinity for the compounds than for ATP. This is consistent with literature and the preliminary results, as the inhibitors were found to have an IC50 in the nanomolar to micromolar range (Stephanie Kim et al., 2020), and the Kd for ATP is 17 µM (Morris et al., 2002).

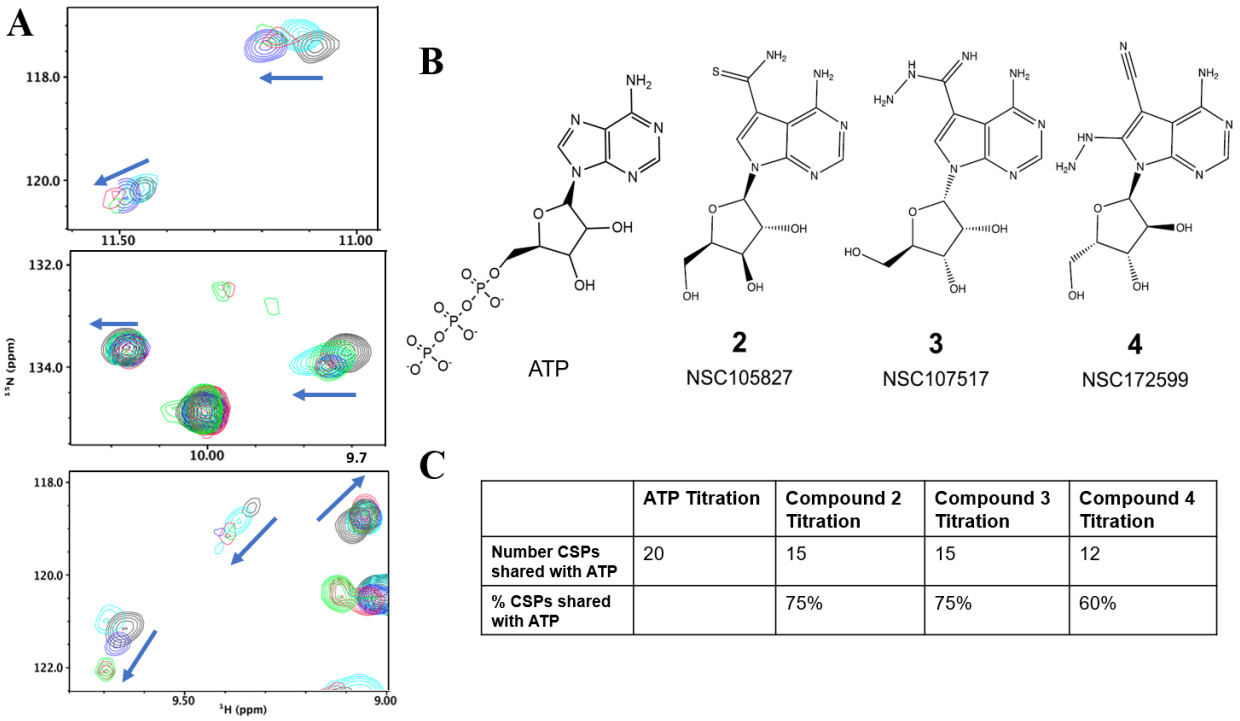

C

	ATP Titration	Compound 2 Titration	Compound 3 Titration	Compound 4 Titration
Number CSPs shared with ATP	20	15	15	12
% CSPs shared with ATP		75%	75%	60%

Figure 16: In all titrations, many of the same peaks experienced significant CSPs. **A**. A collection of peaks in which free CDK2 (black) is overlayed with all titrations: CDK2 with ATP (cyan), compound 2 (blue) , compound 3 (red), and compound 4 (green). The titrated peaks displayed significant CSPs. Arrows display the general direction of the CSPs from the free CDK2 spectra. **B.** The chemical structures of ATP and the 3 compounds. The 3 compounds have similar chemical structures to ATP, with a 2-ring base and pentose forming the main structure. **C.** Many of the peaks experiencing CSPs were uniform in all the compounds tested. The 20 most significant chemical shift perturbations in the ATP titration were compared with the compound titrations. The percentage of shared chemical shift perturbations are listed.

5. Conclusion

In conclusion, while CDK2 was purified successfully, the aggregation of MBP-CyclinA2 made it impossible to test the effect of the inhibitors on independent CyclinA2, or the CDK2-CyclinA2 complex. CDK2 has interactions with compounds 2, 3, and 4. The similarities in which peaks experienced amide chemical shift perturbations when compared to the ATP titration suggests that these compounds competitively inhibit the ATP binding site. Additionally, the inhibitors, specifically compound 2, appear to cause larger chemical shift perturbations than ATP, indicating that CDK2 may bind more tightly to the inhibitors. Currently, none of these compounds are labeled as being CDK2 inhibitors in the NSC database. In a broader pharmacological perspective, these compounds may not be as therapeutically promising as inhibitors which interact with the CDK2 allosteric site, as the ATP binding cleft is highly conserved in the CDK family, and specificity would be limited. However, this high degree of homology suggests that these compounds may also be inhibitory to other members of the CDK family.

While these inhibitors interact with CDK2, it is unclear whether they also act by binding to the allosteric site on CyclinA2, or to the CyclinA2-CDK2 complex. Furthermore, it is unknown how compound 1 interacts with CDK2, as it was not tested. Structurally, compound 1 is not as similar to ATP compared to compounds 2, 3, and 4 (Figure 3), so it would be interesting to determine if CDK2 interacts with it in a similar fashion.

6. References

1. Abraham, R. J., Byrne, J. J., Griffiths, L., & Perez, M. (2006). 1H chemical shifts in NMR: Part 23, the effect of dimethyl sulphoxideversus chloroform solvent on1H chemical shifts. *Magnetic Resonance in Chemistry*, *44*(5), 491–509. https://doi.org/10.1002/mrc.1747

2. Bao, Z. Q., Jacobsen, D. M., & Young, M. A. (2011). Briefly bound to activate: Transient binding of a second catalytic magnesium activates the structure and dynamics of CDK2 kinase for catalysis. *Structure*, *19*(5), 675–690. https://doi.org/10.1016/j.str.2011.02.016

3. Brown, N. R., Noble, M. E. M., Endicott, J. A., & Johnson, L. N. (1999). The structural basis for specificity of substrate and recruitment peptides for cyclin-dependent kinases. *Nature Cell Biology*, *1*(7), 438–443. https://doi.org/10.1038/15674

4. Desai, D., Wessling, H. C., Fisher, R. P., & Morgan, D. O. (1995). Effects of Phosphorylation by CAK on Cyclin Binding by CDC2 and CDK2. In *MOLECULAR AND CELLULAR BIOLOGY* (Vol. 15, Issue 1).

5. Faber, E. B., Tian, D., Burban, D., Levinson, N. M., Hawkinson, J. E., & Georg, G. I. (2020). Cooperativity between Orthosteric Inhibitors and Allosteric Inhibitor 8-Anilino-1-Naphthalene Sulfonic Acid (ANS) in Cyclin-Dependent Kinase 2. *ACS Chemical Biology*, *15*(7), 1759–1764. https://doi.org/10.1021/acschembio.0c00169

6. Grigoroudis, A. I., McInnes, C., Premnath, P. N., & Kontopidis, G. (2015). Efficient soluble expression of active recombinant human cyclin A2 mediated by E. coli molecular chaperones. *Protein Expression and Purification*, *113*, 8–16. https://doi.org/10.1016/j.pep.2015.01.013

7. Gygli, P. E., Chang, J. C., Gokozan, H. N., Catacutan, F. P., Schmidt, T. A., Kaya, B., Goksel, M., Baig, F. S., Chen, S., Griveau, A., Michowski, W., Wong, M., Palanichamy, K., Sicinski, P., Nelson, R. J., Czeisler, C., & Otero, J. J. (2016). Cyclin A2 promotes DNA repair in the brain during both development and aging. *Aging*, *8*(7), 1540–1570. https://doi.org/10.18632/aging.100990

8. Hochegger, H., Takeda, S., & Hunt, T. (2008). Cyclin-dependent kinases and cell-cycle transitions: Does one fit all? In *Nature Reviews Molecular Cell Biology* (Vol. 9, Issue 11, pp. 910–916). Nature Publishing Group. https://doi.org/10.1038/nrm2510

9. Jeffrey, P. D., Russo, A. A., Polyak, K., Gibbs, E., Hurwitz, J., Massagué, J., & Pavletich, N. P. (1995). Mechanism of CDK activation revealed by the structure of a cyclinA-CDK2 complex. *Nature*, *376*(6538), 313–320. https://doi.org/10.1038/376313a0

10. Kanakkanthara, A., Jeganathan, K. B., Limzerwala, J. F., Baker, D. J., Hamada, M., Nam, H. J., Van Deursen, W. H., Hamada, N., Naylor, R. M., Becker, N. A., Davies, B. A., Van Ree, J. H., Mer, G., Shapiro, V. S., Maher, L. J., Katzmann, D. J., & Van Deursen, J. M. (2016).

Cyclin A2 is an RNA binding protein that controls Mre11 mRNA translation. *Science*, *353*(6307), 1549–1552. https://doi.org/10.1126/science.aaf7463

11. Kapust, R. B., & Waugh, D. S. (1999). Escherichia coli maltose-binding protein is uncommonly effective at promoting the solubility of polypeptides to which it is fused . *Protein Science*, *8*(8), 1668–1674. https://doi.org/10.1110/ps.8.8.1668

12. Li, Y., Zhang, J., Gao, W., Zhang, L., Pan, Y., Zhang, S., & Wang, Y. (2015). Insights on structural characteristics and ligand binding mechanisms of CDK2. In *International Journal of Molecular Sciences* (Vol. 16, Issue 5, pp. 9314–9340). MDPI AG. https://doi.org/10.3390/ijms16059314

13. Liu, Q., Gao, J., Zhao, C., Guo, Y., Wang, S., Shen, F., Xing, X., & Luo, Y. (2020). To control or to be controlled? Dual roles of CDK2 in DNA damage and DNA damage response. In *DNA Repair* (Vol. 85, p. 102702). Elsevier B.V. https://doi.org/10.1016/j.dnarep.2019.102702

14. Morris, M. C., Gondeau, C., Tainer, J. A., & Divita, G. (2002). Kinetic mechanism of activation of the Cdk2/cyclin A complex: Key role of the C-lobe of the Cdk. *Journal of Biological Chemistry*, *277*(26), 23847–23853. https://doi.org/10.1074/jbc.M107890200

15. Otero, J. J., Kalaszczynska, I., Michowski, W., Wong, M., Gygli, P. E., Gokozan, H. N., Griveau, A., Odajima, J., Czeisler, C., Catacutan, F. P., Murnen, A., Schüller, U., Sicinski, P., & Rowitch, D. (2014). Cerebellar cortical lamination and foliation require cyclin A2. *Developmental Biology*, *385*(2), 328–339. https://doi.org/10.1016/j.ydbio.2013.10.019

16. Stephanie Kim, B. S., Lindert, S., & José Otero William Ray Sherwin Singer, A. C. (n.d.). *Structure-based Computer Aided Drug Discovery: Applications for Polypharmacology*.

17. Urban, P. L. (2016). Quantitative mass spectrometry: An overview. In *Philosophical Transactions of the Royal Society A: Mathematical, Physical and Engineering Sciences* (Vol. 374, Issue 2079). Royal Society of London. https://doi.org/10.1098/rsta.2015.0382

18. Vandenbosch, R., Borgs, L., Beukelaers, P., Foidart, A., Nguyen, L., Moonen, G., Berthet, C., Kaldis, P., Gallo, V., Belachew, S., & Malgrange, B. (2008). *Cell Cycle CDK2 is Dispensable for Adult Hippocampal Neurogenesis CDK2 is Dispensable for Adult Hippocampal Neurogenesis*. https://doi.org/10.4161/cc.6.24.5048

19. Waugh, D. S. (2016). The remarkable solubility-enhancing power of Escherichia coli maltose-binding protein. In *Postepy biochemii* (Vol. 62, Issue 3, pp. 377–382).